

Halogen Bonding in the Gas Phase: A Comparison of the Iodine Bond in $B \cdots ICl$ and $B \cdots ICF_3$ for Simple Lewis Bases B

J. Grant Hill, Anthony C. Legon, David P. Tew, and Nicholas R. Walker

Abstract Methods for observing the rotational spectra of the halogen-bonded complexes $B \cdots ICl$ and $B \cdots ICF_3$ ($B = N_2$, CO, $HC \equiv CH$, $H_2C = CH_2$, H_2O , H_2S , PH_3 or NH_3) and deriving from them properties such as angular geometry, radial geometry, the strength of the intermolecular bond, and the extent of electron redistribution on complex formation are described. Comparison of various properties reveals several similarities between the two series. Thus, the $B \cdots ICF_3$ obey a set of rules which were originally proposed to rationalise the angular geometries of hydrogen-bonded complexes of the type $B \cdots HX$, but which were subsequently found to apply to their halogen-bonded analogues $B \cdots XY$, where XY is a dihalogen molecule, including ICl . Important for establishing the validity of these rules in both series $B \cdots ICl$ and $B \cdots ICF_3$ were the complexes with $B = H_2O$ or H_2S . The configuration at O in $H_2O \cdots ICF_3$ and $H_2O \cdots ICl$ is effectively planar. On the other hand, the configuration at S in $H_2S \cdots ICF_3$ and $H_2S \cdots ICl$ is permanently pyramidal. Ab initio calculations of potential energy functions for inversion at O or S performed at the CCSD(T)(F12*)/cc-pVDZ-F12 level of theory confirmed these conclusions. Comparison of the intermolecular stretching force constants k_σ show that the series $B \cdots ICF_3$ is systematically more weakly bound than $B \cdots ICl$. Interpretation of k_σ in terms of nucleophilicities N_B of B and electrophilicities E_{IR} of ICl and ICF_3 reveals that $E_{ICF_3} \approx E_{ICl}/3$. Experimental and ab initio values of distances $r(Z \cdots I)$, where Z is the acceptor atom/

J.G. Hill

Department of Chemistry, University of Sheffield, Sheffield S3 7HF, UK
e-mail: grant.hill@sheffield.ac.uk

A.C. Legon (✉) and D.P. Tew

School of Chemistry, University of Bristol, Bristol BS8 1TS, UK
e-mail: a.c.legon@bristol.ac.uk; david.tew@bristol.ac.uk

N.R. Walker

School of Chemistry, Bedson Building, Newcastle University, Newcastle-upon-Tyne NE1 7RU, UK
e-mail: nick.walker@newcastle.ac.uk

region of B, show that, for a given B, the intermolecular bond of $B \cdots ICF_3$ is longer than that of $B \cdots ICl$. The electronic charge redistributed from B to ICF_3 on formation of $B \cdots ICF_3$ is probably negligibly small.

Keywords Ab initio calculations · Angular and radial geometry · Intermolecular force constants · Iodine bond · Iodine monochloride · Iodo-trifluoromethane · Lewis bases · Potential energy functions · Rotational spectroscopy

Contents

- 1 Introduction
- 2 Methods of Observing Rotational Spectra of Complexes $B \cdots ICl$ and $B \cdots ICF_3$
 - 2.1 Pulsed-Jet, Fourier-Transform Microwave Spectroscopy Conducted in a Fabry–Perot Cavity
 - 2.2 Chirped-Pulse, Fourier-Transform Microwave Spectroscopy
- 3 Molecular Properties of $B \cdots ICl$ and $B \cdots ICF_3$ Available from Spectroscopic Constants Obtained from Analysis of Rotational Spectra
 - 3.1 Geometry from Rotational Constants
 - 3.2 Intermolecular Stretching Force Constant k_σ from Centrifugal Distortions Constants
 - 3.3 Electric Charge Redistribution on Formation of $B \cdots ICl$ from I and Cl Nuclear Quadrupole Coupling Constants
- 4 Comparison of Observed Properties of $B \cdots ICl$ and $B \cdots ICF_3$
 - 4.1 Angular Geometry: Do Complexes $B \cdots ICF_3$ Obey the Rules?
 - 4.2 Radial Geometry: How Do the Halogen Bond Distances $Z \cdots I$ Vary from $B \cdots ICl$ to $B \cdots ICF_3$?
 - 4.3 Intermolecular Stretching Force Constants k_σ : How Does Replacement of Cl in $B \cdots ICl$ by CF_3 Change the Electrophilicity of the Halogen Bond Donor Molecule?
 - 4.4 Electric Charge Rearrangement on Formation of $B \cdots ICl$ and $B \cdots ICF_3$ Complexes

Conclusions

References

1 Introduction

This chapter compares the gas-phase properties of two groups of binary complexes, in both of which the components are held together by means of an iodine bond. The two groups of complexes are of the general type $B \cdots I-R$, where B is one of a range of simple Lewis bases and R is either the atom Cl [1–9] or the group CF_3 [10–16]. Some generalisations appropriate to both groups are discussed.

Only relatively small complexes in which the components are linked by a halogen bond have been investigated in the gas phase. In particular, only those of the type $B \cdots X-R$, where B is a simple Lewis base, X is the atom forming the halogen bond to the acceptor atom/centre Z of B, and R is either another halogen atom [17–20] or the groups CF_3 [10–16, 21–23], have been examined spectroscopically. Among the $B \cdots XCF_3$ groups, the series with $X=I$ is the most extensive and is the focus of this chapter. The technique predominantly employed for gas-phase

studies has been microwave spectroscopy, which is conducted under conditions where the complexes $B \cdots X-R$ can be investigated in effective isolation, unperturbed by either the solvent or lattice effects that are present in condensed phases. In the work described here, the results are derived from pure rotational spectra, which are usually observed in the microwave region. Also related to the content of this chapter are the systematic investigations of the vibrational spectra of complexes of the type $B \cdots XCF_3$ when dissolved in liquid noble gases (described in chapter “Infrared and Raman measurements of halogen bonding in cryogenic solutions”). The solvent–solute interactions are then present but small. Recently, Bevan et al. have carried out some very high-resolution vibration-rotation spectroscopy of gas-phase, halogen-bonded complexes such as $OC \cdots Cl_2$ [24] by using quantum cascade lasers.

Analysis of rotational spectra provides very precise spectroscopic constants which can be interpreted to give various properties of the isolated complexes $B \cdots X-R$, and therefore such properties are the most appropriate for comparison with the results of ab initio electronic structure calculations. The series of halogen-bonded complexes involving Lewis bases with dihalogen molecules $B \cdots XY$ ($XY = F_2, ClF, Cl_2, BrCl, Br_2$ or ICl) is, so far, the series most completely characterised by means of rotational spectroscopy; this work is conveniently summarised in [18]. An advantage of dihalogens acting as the halogen-bond donor lies in the absence (for F_2, Cl_2 and Br_2) or sparseness (for $ClF, BrCl$ and ICl) of their rotational spectra. Comparisons of the way derived properties change as first B and then XY are systematically varied have led to some generalisations about the halogen bond [25–30]. These generalisations are concerned with the geometry of the complex, the strength of its intermolecular bond and, in suitable cases, the extent of the electric charge rearrangement that accompanies complex formation. Examples of these generalisations are some rules for the interpretation and prediction of angular geometry [18] (i.e. the relative orientation of the B and XY subunits within $B \cdots XY$) and an expression which allows the prediction of the intermolecular stretching force constant k_σ (one measure of the strength of the interaction of B and XY) from properties assigned to the isolated molecules B and XY , namely the nucleophilicity N_B of B and the electrophilicity E_{XY} of XY [18, 28]. The experimental results and generalisations for $B \cdots XY$ have been thoroughly reviewed elsewhere [17–20]. In these reviews, attention was drawn to a set of identical generalisations previously developed from investigations of the rotational spectra of hydrogen-bonded complexes $B \cdots HX$ in which both B and X were systematically varied. This parallelism between the hydrogen bond and the halogen bond suggests a common origin for these two types of interaction, but such a conclusion must be tempered with caution [31].

The rotational spectra of the halogen-bonded complexes $B \cdots XCF_3$ having a trifluorohalogenomethane XCF_3 as the X donor [10–16, 21–23] have been observed and analysed more recently than those in which a dihalogen molecule XY is the halogen-bond donor, this order being dictated, at least in part, by an instrumental development discussed in Sect. 2.2. Of the series of $B \cdots XCF_3$ complexes, the one to be discussed here involves $X = I$ as the halogen donor atom and $B = N_2, CO$,

$\text{HC}\equiv\text{CH}$, $\text{H}_2\text{C}=\text{CH}_2$, H_2O , H_2S , PH_3 or NH_3 as the Lewis bases. The reason for the particular interest in ICF_3 lies in its role as the tractable prototype for those molecules, such as tetrafluoro-diiodobenzene, employed in crystal engineering applications of the halogen bond [32]. The multiple fluorination is used as a means of withdrawing electrons from the I atom, thereby enhancing the strength of the halogen bond that it forms. In this chapter, we take the opportunity to compare the results for the series $\text{B}\cdots\text{ICF}_3$ with those of the corresponding series $\text{B}\cdots\text{ICl}$, to examine the extent to which replacement of Cl by CF_3 affects the iodine bond, and to find out whether the generalisations previously identified for the latter group of complexes also apply to the former.

The structure of the remainder of this chapter is as follows. In Sect. 2, the two methods used to observe the rotational spectra of complexes $\text{B}\cdots\text{ICl}$ and $\text{B}\cdots\text{ICF}_3$ are briefly outlined, namely pulsed-jet, Fourier-transform microwave spectroscopy in a Fabry–Perot cavity (Sect. 2.1), and chirped-pulse, Fourier-transform microwave spectroscopy (Sect. 2.2), with the emphasis on their advantages and disadvantages. Section 3 describes the properties of the $\text{B}\cdots\text{ICl}$ and $\text{B}\cdots\text{ICF}_3$ molecules that can be derived from spectroscopic constants obtained from analysis of rotational spectra, i.e. the geometry from rotational constants (Sect. 3.1), the intermolecular stretching force constant k_σ from centrifugal distortion constants (Sect. 3.2) and the electric charge redistribution on formation of $\text{B}\cdots\text{ICl}$ from the I and Cl nuclear quadrupole coupling constants (Sect. 3.3). The comparison of observed properties of $\text{B}\cdots\text{ICl}$ and $\text{B}\cdots\text{ICF}_3$ is given in Sect. 4 in which we consider (1) whether $\text{B}\cdots\text{ICF}_3$ complexes, as do their $\text{B}\cdots\text{ICl}$ counterparts, obey the rules for angular geometry (Sect. 4.1), (2) radial geometry and in particular how the halogen bond distances $\text{Z}\cdots\text{I}$ vary from $\text{B}\cdots\text{ICl}$ to $\text{B}\cdots\text{ICF}_3$ (Sect. 4.2) and (3) (in Sect. 4.3) whether the intermolecular stretching force constants k_σ for the $\text{B}\cdots\text{ICF}_3$ series allow an electrophilicity E_{ICF_3} to be determined for ICF_3 and, if so, how replacement of $\text{R} = \text{Cl}$ by CF_3 affects the electrophilicity of the halogen donor molecule. A brief argument to establish that the extent of electric charge rearrangement on formation of $\text{B}\cdots\text{ICF}_3$ complexes from B and ICF_3 is probably very small is given in Sect. 4.4. Section “Conclusions” presents a summary of the conclusions.

2 Methods of Observing Rotational Spectra of Complexes $\text{B}\cdots\text{ICl}$ and $\text{B}\cdots\text{ICF}_3$

Two methods [33–36], having several features in common, have been used to observe the rotational spectra of complexes of the type $\text{B}\cdots\text{ICl}$ and $\text{B}\cdots\text{ICF}_3$. Both employ supersonic expansion of a mixture of B and I–R diluted in an inert gas (argon) to produce a short gas pulse (≈ 1 ms duration) containing a sufficient number density of the complexes $\text{B}\cdots\text{I–R}$ which then expand into a vacuum chamber. The important properties of the supersonic expansion in this context are

(1) that the $B \cdots I-R$ molecules so formed rapidly achieve collisionless expansion in the chamber with an effective translational temperature of only ≈ 1 K, so that even very weakly bound complexes survive until the gas pulse collides with part of the vacuum chamber/pumping system, and (2) that complexes are usually in their vibrational ground state (unless very low energy vibrational states such as those caused by hindered rotation exist) and in their lower energy rotational states. Both techniques then involve the polarization of rotational transitions in a macroscopic ensemble of molecules $B \cdots IR$ by means of a short pulse of microwave radiation, both recording the amplitude of the spontaneous coherent emission from the polarized ensemble as a function of time (time-domain experiment) after the polarizing radiation has decayed sufficiently in intensity that there is no significant background radiation against which to discriminate. Both employ Fourier transformation of the time-domain signal, usually to yield the intensity vs frequency spectrum. In both, the physics of the creation of the macroscopic polarization and its decay are very similar to that involved in the NMR experiment, the main differences being (1) that the microwave experiment involves an electric polarization while the NMR experiment relies on a magnetic polarization and (2) that the decay of the electric polarization is much faster ($T_2 \approx 100$ μ s) than that of the magnetic polarization ($T_2 \approx 10$ s). Each technique has Fourier-transform microwave spectroscopy in its title, but they differ in the frequency bandwidth of the polarizing microwave pulse. An outline of each technique is given below, with emphasis on their differences, together with an indication of their advantages and disadvantages.

2.1 Pulsed-Jet, Fourier-Transform Microwave Spectroscopy Conducted in a Fabry–Perot Cavity

The essential features of the pulsed-jet, Fourier-transform, Fabry–Perot (F–P) cavity technique [33, 34] are as follows. A short pulse (duration ≈ 1 –2 ms) of the gas mixture (usually about 1% each of B and I–R in argon at a total pressure of 2 bar) is produced by a solenoid valve and enters an evacuated microwave F–P cavity along its axis. The F–P cavity consists of a pair of confocal, spherical aluminium mirrors having a high Q and an acceptance bandwidth of ≈ 1 MHz. After a suitable delay to allow the gas pulse to arrive at the centre of the mirrors, monochromatic microwave radiation (produced by a microwave synthesizer) is formed into a pulse of ≈ 1 μ s duration and carries with it into the F–P cavity a range of frequencies covering about 1 MHz, thereby matching the cavity bandwidth. The microwave pulse, if of sufficient power, can therefore polarize all rotational transitions of the target molecules whose frequencies fall within approx. 1 MHz of the frequency to which the Fabry–Perot cavity is tuned. After a short delay to ensure that the polarizing microwave pulse has decayed, the spontaneous coherent emission from the rotationally polarized gas is recorded in the time domain, Fourier

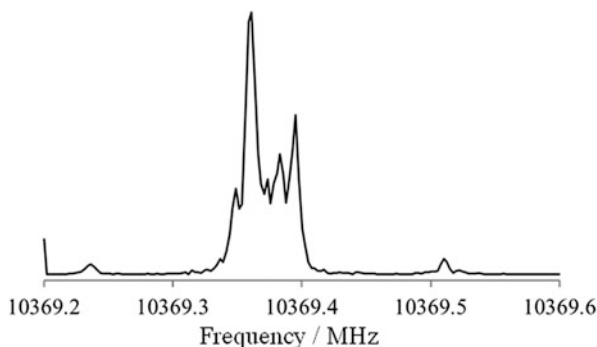


Fig. 1 A small part of the nuclear quadrupole hyperfine structure of the $J=6 \rightarrow 5$, $K=0 \rightarrow 0$ transition of $\text{H}_3^{14}\text{N} \cdots ^{127}\text{ICF}_3$ recorded with a pulsed-jet, F-T microwave spectrometer incorporating a Fabry–Perot cavity. The feature at 10,369.365 MHz is a combination of the $F_1=3.5 \rightarrow 4.5$, $F_2=2.5 \rightarrow 3.5$ and the $F_1=3.5 \rightarrow 4.5$, $F_2=4.5 \rightarrow 5.5$ hyperfine components (each appearing as a Doppler doublet) arising from the presence of the ^{127}I and ^{14}N nuclei in the molecule. The spectrum is the average of the signals collected from 11,500 gas pulses

transformed and the power spectrum displayed. The parallel propagation of the gas and microwave pulses along the cavity axis leads to a so-called Doppler doublet (the centre frequency of which is the transition frequency), but has the advantage that it reduces the full-width at half-maximum intensity of each component to approx. 5 kHz. This instrument therefore has a very high resolution and a correspondingly high accuracy of frequency measurement (typically 0.5 kHz). In addition, only a relatively low microwave power is needed to polarize rotationally a large fraction of the gas pulse when within the F–P cavity and this ensures a high sensitivity. Disadvantages include (1) slow searching because every time the radiation is changed (usually in 0.5 MHz steps to ensure no transitions are missed) the cavity must be re-tuned to the radiation frequency and (2) difficulty in extracting relative intensities because the intensity of an observed signal depends critically on the mode of the F–P cavity in use and on the how far the radiation is offset from the exact resonant frequency of the cavity. As an example of the resolution and sensitivity, part of the extensive hyperfine structure arising from coupling of the ^{14}N and ^{127}I nuclear spins to the overall rotational angular momentum in the $J=6 \rightarrow 5$ transition of $\text{H}_3^{14}\text{N} \cdots ^{127}\text{IF}_3$ is shown in Fig. 1. Each transition is split into a doublet by the Doppler effect mentioned earlier.

2.2 Chirped-Pulse, Fourier-Transform Microwave Spectroscopy

The sequence of events comprising a gas pulse, microwave pulse, detection of the spontaneous coherent emission and Fourier-transformation of the detected radiation

is also used in the chirped-pulse version of FTMW spectroscopy. Chirped-pulse (CP) FTMW spectroscopy [35, 36] additionally entails the use of a microwave polarization pulse which is rapidly swept over a very broad frequency range. Such experiments have only recently become possible as a result of advances in the technology available for the digital generation and processing of waveforms. Compared with typical FTMW experiments exploiting an F–P cavity, the polarization pulse duration is unchanged. However, a pulse of significantly higher intensity must be used to polarize efficiently molecules across the broader bandwidth of the experiment. The intensity required in the chirped polarization pulse is directly proportional to its bandwidth.

When implemented within a spectrometer that exploits fixed-frequency microwave pulses (i.e. of the type described in Sect. 2.1), a Fabry–Perot cavity comprising confocal, spherical mirrors allows higher sensitivity and resolution than could otherwise be achieved. However, the acceptance bandwidth of such a cavity is too narrow to gain any advantage when a microwave polarization pulse spanning 12 GHz in frequency is used. For this reason, the polarizing pulse is introduced and the molecular emission detected using broadband horn antennae in a chirped-pulse FTMW spectrometer. The principal advantage of the CP-FTMW technique undoubtedly arises from the opportunity to excite all transitions across a broad bandwidth in a single measurement. At microwave frequencies, all transitions between 6 and 18 GHz can be probed simultaneously, representing a very significant expansion of the frequency range which can be probed compared with experiments that exploit a Fabry–Perot cavity. An additional, related advantage arises because the intensity of the chirped pulse in a CP-FTMW spectrometer is highly uniform across the frequency range under examination. It is thus easier to compare the relative intensities of different transitions across a broad frequency range. The intensities of transitions measured by FTMW experiments exploiting a Fabry–Perot cavity are dependent on a greater range of factors, as described in Sect. 2.1. Figure 2 shows a recording of the rotational spectrum of $\text{H}_3\text{N} \cdots \text{ICF}_3$ observed with the CP-FTMW spectrometer when the frequency range displayed is successively decreased. A small part of the same spectrum recorded with a spectrometer of the type discussed in Sect. 2.1 is shown in Fig. 1. The smaller line widths and accompanying increased resolution are apparent.

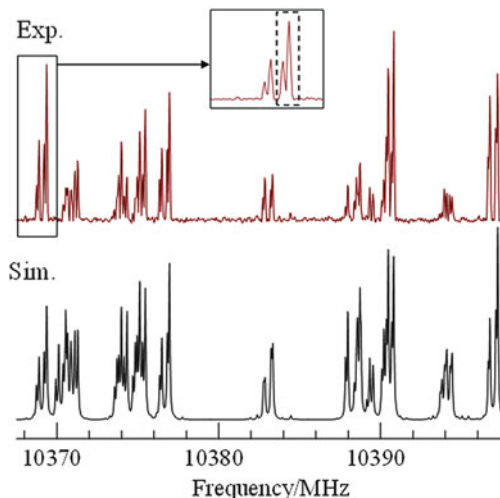


Fig. 2 Part of the $J=6 \rightarrow 5$ transition of $\text{H}_3^{14}\text{N} \cdots ^{127}\text{ICF}_3$ recorded with a chirped-pulse F-T microwave spectrometer in the frequency range 10,365–10,400 MHz is shown in the *upper panel* while the *lower panel* is a simulation obtained with the aid of the spectroscopic constants given in [15]. A small section of the spectrum is expanded within the *inset*. The features at 10,369.365 MHz, further expanded and enclosed within the *dashed box*, are those displayed in Fig. 1. The spectrum resulted from the averaging of the signals from 13,000 gas pulses

3 Molecular Properties of $\text{B} \cdots \text{ICl}$ and $\text{B} \cdots \text{ICF}_3$ Available from Spectroscopic Constants Obtained from Analysis of Rotational Spectra

The techniques discussed in Sects. 2.1 and 2.2 lead to the rotational spectra of the $\text{B} \cdots \text{I-R}$ ($\text{R} = \text{Cl}$ or CF_3) complexes of good intensity but usually in their ground vibrational states only. Sometimes, however (with $\text{H}_3\text{N} \cdots \text{ICF}_3$, $\text{H}_2\text{O} \cdots \text{ICF}_3$, for example), the corresponding spectra in excited internal rotation states are also observed. Here we shall be concerned only with molecular properties pertaining to vibrational ground states. Analysis of the ground-state spectra lead to ground-state spectroscopic constants, among which are included rotational constants, centrifugal distortion constants and nuclear quadrupole coupling constants. The spectroscopic constants can be interpreted, at various levels of approximation, to give properties of the complexes with which they are associated. These properties and the approximations involved in obtaining them are discussed in Sects. 3.1, 3.2 and 3.3.

3.1 Geometry from Rotational Constants

Ground-state rotational constants A_0 , B_0 and C_0 are simply related to the zero-point principal moments of inertia I_a^0 , I_b^0 and I_c^0 through the equations $A_0 = h/8\pi^2 I_a^0$,

$B_0 = h/8\pi^2 I_b^0$ and $C_0 = h/8\pi^2 I_c^0$, where a , b and c delineate the three principal inertia axes. The principal moments of inertia associated with the equilibrium geometry (indicated by a superscript e) are simple functions of only the masses and the equilibrium principal-axis coordinates of the atoms. The expression for the equilibrium principal moment of inertia I_a^e , for example, is just $I_a^e = \sum_i m_i (b_i^2 + c_i^2)$,

with corresponding expressions for I_b^e and I_c^e . If an isotopic substitution is made at a particular atom, the changes ΔI_a^e , ΔI_b^e and ΔI_c^e in the moments of inertia which accompany the substitution are related by exact equations (called Kraitchman's equations [37]) to the principal-axis coordinates of the atom in question. Isotopic substitution at each atom in turn thus leads to a complete geometry for the molecule.

Unfortunately, equilibrium moments of inertia are very rarely available experimentally, except for the simplest of molecules and certainly not for weakly bound complexes such as those under discussion here. The approach usually adopted then is to use zero-point moments of inertia as if they were equilibrium values. When isotopic substitutions are made and the geometry is fitted to the minimum number of zero-point moments of inertia by the least-squares method, the result is called an r_0 geometry. Since isotopic substitution changes the zero-point motion, the geometry obtained varies depending on the isotopologues chosen, and therefore inconsistencies occur when r_0 geometries are over-determined, i.e. determined from different sets of isotopologues. When changes in zero-point moments of inertia ΔI_a^0 , ΔI_b^0 and ΔI_c^0 are used in Kraitchman's equations [37] in place of equilibrium values (ΔI_a^e , ΔI_b^e , ΔI_c^e), however, the resulting coordinates are referred to as substitution coordinates and the geometry as the r_s geometry [38]. The advantage of r_s geometries is that they exhibit greater internal consistency when over-determined and are closer to equilibrium values than r_0 geometries (for diatomic molecules there is an exact relation $r_s = (r_e + r_0)/2$). Even r_s geometries are not available for the type of molecules considered here, however. In view of the weak intermolecular binding, it is usually assumed that the geometry of each of the two component molecules B and I-R is unperturbed by complex formation. The parameters defining the separation of the two subunits B and I-R and their relative orientation in space, i.e. the radial and angular geometries of the complex, respectively, are obtained by a least-squares fit of the zero-point moments of inertia of the various isotopologues. All molecular geometries of B...I-R considered here are of this pseudo- r_0 type.

3.2 Intermolecular Stretching Force Constant k_σ from Centrifugal Distortions Constants

Chemical bonds are elastic and, therefore, when a molecule is in its zero-point vibrational state and a rotational state having a quantum number $J > 0$ (i.e. it is rotating), the bonds distort. The higher the rotational energy (i.e. the higher J), the larger the distortion and therefore the geometry changes (very slightly) with the rotational state. In the usual expressions for the energy of rotation of a molecule in

its zero-point state, the main part of the energy is expressed in terms of the zero-point rotational constants A_0 , B_0 and C_0 (often referred to as the effective rigid rotor energy) while the centrifugal distortion contribution is described by small additional terms consisting of centrifugal distortion constants which multiply simple functions of the rotational quantum number J for diatomic and linear molecules or quantum numbers J and K for symmetric-top molecules [39]. The expressions for asymmetric-top molecules are more complicated but the principles are the same. For a diatomic or linear molecule, this energy expression is simply

$$E(J) = hB_0J(J+1) - hD_JJ^2(J+1)^2, \quad (1)$$

in which the second term on the right-hand side takes account of the change of geometry (and therefore rotational energy) with J . D_J is called the (quartic) centrifugal distortion constant. There are higher order (sextic, etc.) centrifugal distortion constants but these are usually negligible unless the molecule is unusually floppy or very high J value transitions are observed. The expressions for symmetric-top and asymmetric-top molecules contain three and five (quartic) centrifugal constants, respectively, because there are other ways in which such molecules change geometry with rotational state, corresponding to rotations about principal inertia axes other than b . However, the term corresponding to D_J for linear/diatomic molecules is also present for symmetric-top and asymmetric-top molecules. It is given the same symbol D_J in symmetric-top molecules but is labelled Δ_J in the latter group.

To a reasonable approximation, the components of a weakly bound complex (such as one of the $B \cdots I-R$ considered here) may be modelled as a pair of rigid molecules held together by a weak intermolecular bond. In the crudest approximation, B and I-R can be taken as point masses and $B \cdots I-R$ becomes a pseudo-diatomic molecule. Clearly in that case the centrifugal distortion constant depends on only one force constant, namely the intermolecular stretching force constant k_σ . The expression relating k_σ and D_J for a complex $B \cdots I-R$ is simply related to that for a diatomic molecule [40] and is given in the pseudo-diatomic approximation by

$$k_\sigma = 16\pi^2\mu \left[\frac{1}{2}(B+C) \right]^3 / D_J, \quad (2)$$

where $\mu = M_B M_{IR} / (M_B + M_{IR})$ and M_B and M_{IR} are the masses of B and I-R, respectively. A more realistic approximation, made by Millen [41], treats the two component molecules as rigid but takes into account their spatial extension of mass. The expressions are different for different types of molecular rotor. For a symmetric-top complex, such as $H_3N \cdots ICl$ [8], the appropriate expression is

$$k_\sigma = (16\pi^2\mu B^3 / D_J) [1 - B/C_{NH_3} - B/B_{ICl}], \quad (3)$$

in which the rotational constants in the denominators of the expressions in square brackets refer to the indicated free molecules and B is that of the complex. Strictly, these rotational constants should be equilibrium values but it is a good

approximation to use zero-point quantities. When the complex is a planar asymmetric-top molecule of C_{2v} symmetry, for example ethyne $\cdots\text{ICl}$ [3], having rotational constants B and C and the centrifugal distortion constant Δ_J , the expression for k_σ takes the form

$$k_\sigma = (8\pi^2\mu/\Delta_J) [B^3(1-b) + C^3(1-c)], \quad (4)$$

in which $b = (B/B_{\text{C}_2\text{H}_2}) + (B/B_{\text{ICl}})$, $c = (C/B_{\text{C}_2\text{H}_2}) + (C/B_{\text{ICl}})$. The expression given by Millen [41] for planar C_{2v} molecules of this type actually refers to D_J , which was the nomenclature employed in an earlier approach to the centrifugal distortion Hamiltonian than that used in the work reported here. D_J so determined differs from Δ_J by a small term. As a consequence, Millen's expression relating D_J and k_σ differs from Eq. (4) by a small additional term within the square brackets. Here we are concerned only with Δ_J values for asymmetric-top molecules and hence Eq. (4) is appropriate. If the complex is an asymmetric-top molecule such as $\text{C}_2\text{H}_4 \cdots \text{ICl}$ [4], in which ICl lies along the C_2 axis that is perpendicular to the plane of the ethene subunit, Eq. (4) also applies. Millen's original derivations were for complexes in which the Lewis acid is a diatomic or linear molecule, but it is readily shown that Eqs. (3) and (4) also apply when the Lewis acid is a symmetric-top molecule, such as ICF_3 .

3.3 *Electric Charge Redistribution on Formation of $\text{B} \cdots \text{ICl}$ from I and Cl Nuclear Quadrupole Coupling Constants*

It has been shown elsewhere [2, 8] that, in a complex $\text{B} \cdots \text{ICl}$, the iodine and chlorine nuclear quadrupole coupling constants can be interpreted on the basis of a simple model (the Townes–Dailey model [42]) to provide information about the electron redistribution which occurs on formation of the complex from its two components.

Nuclei with a spin quantum number $I \geq 1$ can possess an electric quadrupole moment. Since $I = 3/2$ for ^{35}Cl and $I = 5/2$ for ^{127}I , both nuclei in $\text{XY} = ^{127}\text{I}^{35}\text{Cl}$ are quadrupolar. As a result of the electrostatic interaction of the nuclear electric quadrupole moment \mathbf{Q}_X of nucleus X with any electric field gradient $q_{zz} = \partial^2 V^X / \partial z^2$ existing at that nucleus along the intermolecular axis direction z in the molecule XY , the nuclear spin angular momentum \mathbf{I}_X associated with X couples to the overall rotational angular momentum \mathbf{J} , and similarly for nucleus Y . Only a limited number of orientations of the X and Y nuclear spin axes with respect to z are allowed and each of these corresponds to a different energy of interaction of \mathbf{Q}_X with $\partial^2 V^X / \partial z^2$ and \mathbf{Q}_Y with $\partial^2 V^Y / \partial z^2$. The result is a splitting of the rotational energy levels of XY into several so-called *nuclear quadrupole hyperfine components*. By measuring the resulting nuclear quadrupole hyperfine

structure of the rotational transitions, the nuclear quadrupole coupling constants $\chi_{zz}(\text{X})$ and $\chi_{zz}(\text{Y})$ defined by

$$\chi_{zz}(\text{X}) = eQ_{\text{X}} \left(\partial^2 V^{\text{X}} / \partial z^2 \right), \quad (5)$$

and

$$\chi_{zz}(\text{Y}) = eQ_{\text{Y}} \left(\partial^2 V^{\text{Y}} / \partial z^2 \right), \quad (6)$$

can be determined accurately. Since the proton charge e and the conventional nuclear electric quadrupole moments Q_{X} and Q_{Y} are known constants, Eqs. (5) and (6) lead to the electric field gradients (efgs) at X and Y along the z axis. The efg at a given nucleus X is determined entirely by the electron charge distribution in the molecule XY outside a small sphere surrounding the X nucleus.

The Townes–Dailey model [42] is a simple way of interpreting nuclear quadrupole coupling constants in terms of the electron distribution within the molecule XY. The model makes the following approximations:

1. Filled inner-core electrons associated with an atom remain spherically symmetric when the atom is subsumed into a molecule and therefore the efg at its nucleus remains zero. Thus, only valence electrons contribute to the efg. Of these, s electrons are assumed to remain spherically symmetric when in a molecule and therefore do not contribute.
2. Because the efg at a nucleus arising from a given electron varies with the distance of the electron from the nucleus according to $\langle r^{-3} \rangle$, the contributions to $q_{zz} = \partial^2 V^{\text{X}} / \partial z^2$ from electrons centred on atom Y are neglected.
3. Hence, only p,d,... valence electrons centred on X contribute to $\partial^2 V^{\text{X}} / \partial z^2$. These are, moreover, assumed to be in orbitals unperturbed from the free-atom orbitals. If the contribution of an electron characterised by quantum numbers n, l , and m to the efg in the free atom X is written as $q_{n,l,m}$, and recognising that for a p electron $2q_{n,1,1} = 2q_{n,1,-1} = -q_{n,1,0}$, it follows that, according to the Townes–Dailey approximation, the efg along the z direction at the nucleus of the halogen atom X (electronic configuration np^5) in the molecule XY is just $2q_{n,1,1} + 2q_{n,1,-1} + q_{n,1,0} = -q_{n,1,0}$ which is that arising from an absence of an np_z electron. Clearly, if we define the nuclear quadrupole coupling constant of free atom X as $\chi_{\text{A}}(\text{X}) = -eQ_{\text{X}} q_{n,1,0}^{\text{X}}$, then when the atom X is in the XY molecule, the coupling constant of X is $\chi_{zz}(\text{X}) = -eQ_{\text{X}} q_{n,1,0}^{\text{X}} = \chi_{\text{A}}(\text{X})$ in the Townes–Dailey approximation.

When a complex $\text{B} \cdots \text{XY}$ is formed by bringing up the Lewis base B to XY along the internuclear axis z of XY, the efgs at X and Y change. If we assume that the changes arise from a fraction δ_i of an electron transferred from B into the np_z orbital of X and a fraction δ_p of an electron transferred from X into the np_z orbital of Y, it follows that the nuclear quadrupole coupling constants in the equilibrium (e) geometry of $\text{B} \cdots \text{XY}$ are given by

$$\chi_{zz}^e(X) = \chi_0(X) - (\delta_i - \delta_p)\chi_A(X), \quad (7)$$

and

$$\chi_{zz}^e(Y) = \chi_0(Y) - \delta_p\chi_A(Y), \quad (8)$$





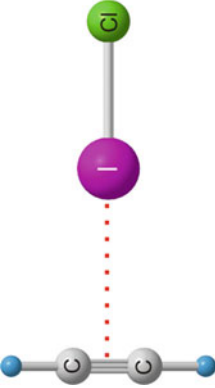
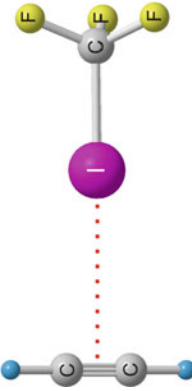
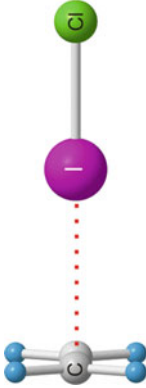
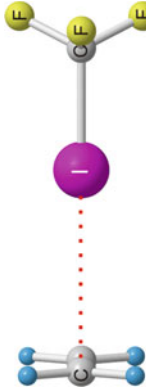


in which $\chi_0(X)$ and $\chi_0(Y)$ are the zero-point coupling constants of the free molecule XY but should strictly be equilibrium values $\chi_e(X)$ and $\chi_e(Y)$. This approximation can be used without introducing significant error, however. It is necessary to modify Eqs. (7) and (8) to allow for the fact that the XY subunit, when within the complex, undergoes zero-point vibrations, particularly an angular oscillation with respect to its centre of mass. These angular oscillations are small for XY = ICl because of the large mass, but the very small corrections of Eqs. (7) and (8) resulting from the motion have been made and are discussed elsewhere [1–9, 19]. Equations (7) and (8) then provide a route to the values of δ_i and δ_p , but only for those complexes in which both X and Y carry quadrupolar nuclei. Such an approach is therefore possible for the complexes $B \cdots ICl$ under discussion in this chapter but not for $B \cdots ICF_3$. Nevertheless, we can use the (mainly small) δ_i for the former series to argue that net intermolecular charge transfer in the latter is probably going to be negligible. The fact that the δ_i values are usually small means that the approximations inherent in the Townes–Dailey model are not too serious here.

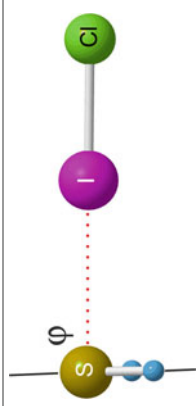
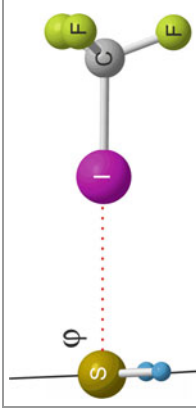
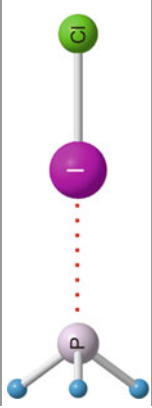

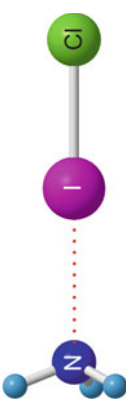

4 Comparison of Observed Properties of $B \cdots ICl$ and $B \cdots ICF_3$

4.1 Angular Geometry: Do Complexes $B \cdots ICF_3$ Obey the Rules?

The angular geometries determined for the two series of complexes $B \cdots ICl$ [1–9] and $B \cdots ICF_3$ [10–16], where $B = N_2, CO, H_2O, C_2H_2, C_2H_4, H_2S, PH_3$ and NH_3 , are shown in Table 1. Each was determined in the approximation that the r_0 geometries of the two separate components are unchanged by complex formation. The species when $B = N_2, CO, PH_3$ and NH_3 are either linear or symmetric-top molecules for both $B \cdots ICl$ and $B \cdots ICF_3$. Therefore their angular geometries are known and, under the approximation mentioned, only the internuclear distances $r_0(Z \cdots I)$ need to be determined to characterise the geometry completely. When $B = C_2H_2$ or C_2H_4 , various observations concerning nuclear spin statistical weight effects and relationships among the principal moments of inertia allow the conclusions that the complex is C_{2v} , T-shaped for $B = C_2H_2$, and that $C_2H_4 \cdots ICl$ has C_{2v} symmetry, with ICl lying along the C_2 axis of C_2H_4 that is perpendicular to the plane containing all the C_2H_4 nuclei. For $B = H_2O$, and H_2S , only the angles defined in each case in Table 1 are necessary in addition to determine the geometry fully, if unperturbed monomer geometries are again assumed. In the case of the $B \cdots ICF_3$

Table 1 Angular geometries of $B \cdots ICl$ and $B \cdots ICF_3$ in the gas phase

$B \cdots ICl$	Point group, Refs.	$B \cdots ICF_3$	Point group, Refs.
	$C_{\infty v}$, [1]		C_{3v} , [10]
	$C_{\infty v}$, [2]		C_{3v} , [11]
	C_{2v} , [3]		Highest symmetry ^a C_s , [12]
	C_{2v} , [4]		Highest symmetry ^a C_s , [13]
	C_s at equilibrium, C_{2v} in zero-point state, $\varphi = 46(2)^\circ$, [5]		Highest symmetry ^a C_s , $\varphi = 34(2)^\circ$, [14]

 <p>Diagram showing the S-Cl-I complex. The sulfur atom (S, yellow) is bonded to two hydrogen atoms (H, white) and a chlorine atom (Cl, green). The iodine atom (I, purple) is bonded to the sulfur atom via a dashed red line representing a halogen bond. The angle between the S-Cl bond and the S-I bond is labeled ϕ.</p>	C_s at equilibrium and in zero-point state. $\phi = 91.9(2)^\circ$, [6]	 <p>Diagram showing the S-F-I complex. The sulfur atom (S, yellow) is bonded to two hydrogen atoms (H, white) and a fluorine atom (F, green). The iodine atom (I, purple) is bonded to the sulfur atom via a dashed red line representing a halogen bond. The angle between the S-F bond and the S-I bond is labeled ϕ.</p>	Highest symmetry ^a C_s , $\phi = 93.7(2)^\circ$, [14]
 <p>Diagram showing the P-Cl-I complex. The phosphorus atom (P, light purple) is bonded to three hydrogen atoms (H, white) and a chlorine atom (Cl, green). The iodine atom (I, purple) is bonded to the phosphorus atom via a dashed red line representing a halogen bond.</p>	C_{3v} [9]	 <p>Diagram showing the P-F-I complex. The phosphorus atom (P, light purple) is bonded to three hydrogen atoms (H, white) and a fluorine atom (F, green). The iodine atom (I, purple) is bonded to the phosphorus atom via a dashed red line representing a halogen bond.</p>	Highest symmetry ^a C_{3v} , [16]
 <p>Diagram showing the N-Cl-I complex. The nitrogen atom (N, blue) is bonded to three hydrogen atoms (H, white) and a chlorine atom (Cl, green). The iodine atom (I, purple) is bonded to the nitrogen atom via a dashed red line representing a halogen bond.</p>	C_{3v} [8]	 <p>Diagram showing the N-F-I complex. The nitrogen atom (N, blue) is bonded to three hydrogen atoms (H, white) and a fluorine atom (F, green). The iodine atom (I, purple) is bonded to the nitrogen atom via a dashed red line representing a halogen bond.</p>	Highest symmetry ^a C_{3v} , [15]

^aThese molecules possess low barriers to internal rotation/other motion. The point group of highest symmetry achieved during the motion is given

series (excluding $B = N_2$ and CO), there is a complication not present in the $B \cdots ICl$ series, namely that in each case there exists a very low potential energy barrier hindering the internal rotation of the CF_3 group against B . Such motion manifests itself in the observed rotational spectra as *vibrational satellites*, in this case rotational spectra in low-lying energy states associated with the hindered internal rotation. The ground-state spectra and the satellites were readily identified in the cases $B = NH_3$ [15] and PH_3 [16] and were analysed according to existing theory for such molecules. Only conclusions drawn from ground-state spectra are discussed here. When $B = H_2O$ [14], C_2H_2 [12], C_2H_4 [13] or H_2S [14] in $B \cdots ICF_3$, a satisfactory theory to account for internal rotation is not available, and it was more difficult to identify the ground-state rotational spectrum. For each, two sets of rotational spectra were observed, one of which could be fitted as a symmetric-top type spectrum while the other was of the expected asymmetric-top type. Each spectral analysis has its own difficulties and the reader is referred to the primary articles for detailed accounts of the fitting process and for detailed methods of interpreting the spectroscopic constants to give the molecular properties. The important point to note in connection with geometry for $B \cdots ICF_3$ for $B = H_2O$, C_2H_2 , C_2H_4 or H_2S is that, whichever of the two types of spectrum was fitted, the geometry obtained was not significantly different.

It is clear from an examination of Table 1 that, for a given B , the pair of complexes $B \cdots ICl$ and $B \cdots ICF_3$ are isomorphic in the sense that they have similar angular geometries. A simple model which accounts for this isomorphism is given below. It is based on a set of empirical rules first proposed for rationalising/predicting angular geometries of hydrogen-bonded complexes $B \cdots HX$ [43–45], but was later extended to include halogen-bonded species [17, 18, 26–30]. The original rules were based on electrostatics in the sense that the electrophilic end δ^+H of the HX molecules is assumed to seek out the most nucleophilic region of B . Nucleophilic regions of B are usually associated with non-bonding electron pairs or π -bonding electron pairs. The rules are as follows:

The angular geometries of hydrogen-bonded complexes $B \cdots HX$ in the gas phase can be predicted by assuming that in the equilibrium conformation the internuclear axis of the HX molecule lies:

1. Along the axis of a non-bonding electron pair (n -pair) carried by B , or
2. Along the local symmetry axis of a π orbital, if B carries no n -pairs or
3. If B carries both n - and π -pairs, rule 1 takes precedence

With these rules, the angular geometries of the hydrogen-bonded complexes $B \cdots HX$, where $X = F, Cl, Br, I, CN$ or CCH , have been rationalised for a wide range of Lewis bases B , as described elsewhere [43–45]. It has also been shown more recently that the rules, when modified by replacing $B \cdots HX$ and HX by $B \cdots XY$ and XY , respectively, also apply to halogen-bonded complexes of the type $B \cdots XY$, in which XY is one of the dihalogen molecules $F_2, ClF, Cl_2, BrCl, Br_2$ or ICl [17, 18]. The range of Lewis bases B investigated was the most extensive in the case of $XY = ClF$ and was similar to that used for the $B \cdots HCl$ series. A close parallelism between the angular geometries of $B \cdots HX$ and $B \cdots XY$ was identified and led to

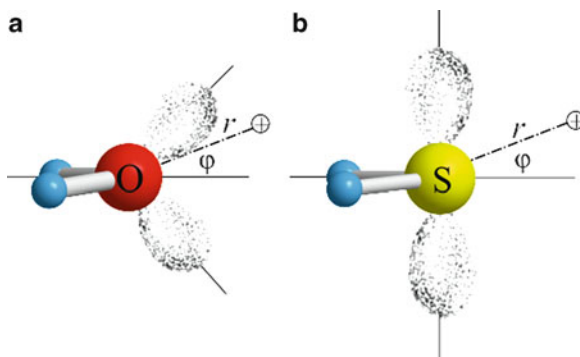


Fig. 3 The chemist's conventional model of the nonbonding electron pairs in (a) H_2O and (b) H_2S . The angle φ is defined in each case as the angle made by a line, of length r , joining a unit positive non-perturbing charge \oplus and the O or S atom with the C_2 axis. The line lies in the plane containing the n -pair axes. r , φ and \oplus are used in the description of the electrostatic potentials shown in Figs. 4 and 5

the proposal [17, 18] of a halogen bond $\text{B} \cdots \text{XY}$ in the gas phase which is the analogue of the more familiar hydrogen bond.

Do these rules apply to complexes formed by halogen bond donors such as ICF_3 as well as by dihalogen molecules XY ? The similarity of the angular geometries of the $\text{B} \cdots \text{ICl}$ and the $\text{B} \cdots \text{ICF}_3$ evident in Table 1 suggests that they do. The angular geometries of $\text{H}_2\text{Z} \cdots \text{ICl}$ and $\text{H}_2\text{Z} \cdots \text{ICF}_3$ when Z is either O or S are particularly important in establishing this result, as indeed were the angular geometries of $\text{H}_2\text{Z} \cdots \text{HX}$ and $\text{H}_2\text{Z} \cdots \text{XY}$ in first formulating the rules for the hydrogen bond and the halogen bond. Given simple electronic models of H_2O and H_2S , the rules also provide an explanation of why the complexes $\text{H}_2\text{S} \cdots \text{HX}$ [45] and $\text{H}_2\text{S} \cdots \text{XY}$ [18] (including $\text{XY} = \text{ICF}_3$ [14]) are permanently pyramidal on the microwave timescale, while their H_2O analogues [14, 18, 45] are inverting and effectively planar.

In the electronic model of H_2O , we assume sp^3 hybridisation of the 2s and 2p orbitals of O. A diagram of this model of H_2O is shown in Fig. 3a and has been drawn with the exaggerated n -pair electron density distributions frequently employed in chemistry. This familiar approach accounts for an HOH angle that is not far from tetrahedral and it implies a similar angle between the axes of the two n -pairs carried by O, which therefore requires an angle φ (see Table 1 for definition of the angle φ) close to 50° for $\text{H}_2\text{O} \cdots \text{HX}$ and $\text{H}_2\text{O} \cdots \text{XY}$ complexes. On the other hand, to explain the HSH angle close to 90° in free H_2S , we might invoke S–H bonds formed by overlap of two 3p orbitals ($3p_x$ and $3p_y$, say) on S with 1s orbitals of H and then place each n -pair in a sp hybrid orbital formed from 3s and $3p_z$ on S. Such a model then requires an angle of 180° between the n -pairs on S, and consequently an angle φ close to 90° (see Fig. 3b and Table 1). Moreover, the larger angle implies a much wider potential energy barrier to inversion of the configuration at S in $\text{H}_2\text{S} \cdots \text{HX}$ and $\text{H}_2\text{S} \cdots \text{XY}$ than that at O in $\text{H}_2\text{O} \cdots \text{HX}$ and $\text{H}_2\text{O} \cdots \text{XY}$. Alternatively, in an unhybridised model for H_2S , one n -pair is viewed as occupying a $3p_z$ orbital while the other occupies the 3s orbital. If the weak interaction is via the n -pair in $3p_z$, the geometrical consequences are identical to those of the hybridised version.

It was pointed out some time ago [45] that this difference in the n -pair angular electron density distributions of H_2O and H_2S is consistent with simple electrostatics. The electric charge distribution of a molecule can be accurately described by sets of point multipoles (charges, dipoles and quadrupoles) placed on atoms and sometimes at the centres of bonds. The values of the multipoles are determined by a *distributed multipole analysis*, as proposed by Stone [46], of the ab initio wavefunction of the molecule. Buckingham and Fowler [47] have provided accurate electric charge distributions for H_2O and H_2S by using this approach. Once the DMA is available, it is straightforward to calculate the electrostatic potential, electric field, etc. at any point outside the molecule in question (by using the **T** tensor formalism set out by Buckingham [48]) without any of the convergence problems experienced when the molecular electric moments are used instead of the DMA to describe the charge distribution. Figure 4 shows the electrostatic potential (the potential energy of a non-perturbing, unit point positive charge \oplus) $V(\varphi)$ plotted against the angle φ (as defined in Fig. 3a) at each of two distances ($r = 1.50$ and 1.75 Å) of \oplus from the O atom. The unit charge \oplus lies at all times in the plane of the n -pair axes and is kept at a fixed distance from the oxygen atom of H_2O . The distance $r = 1.50$ Å is similar to that of the $\delta^+\text{H}$ atom of HF from O in the complex $\text{H}_2\text{O} \cdots \text{HF}$. Figure 4 shows that the electrostatic potential $V(\varphi)$ for $r = 1.50$ Å has two minima at φ ca. $\pm 45^\circ$, i.e. at approximately the angle defined by the n -pair axis directions, and has a low barrier at the planar ($\varphi = 0$) arrangement. The minima deepen and separate as r decreases. The reasons why the minima in the energy do not occur closer to the $\pm 54^\circ$ required by a tetrahedral disposition of electron pairs in H_2O are understood and have been discussed elsewhere [45]. As r increases to 1.75 Å, the minima draw together and the barrier height decreases rapidly but is still non-zero. The results of applying the same procedure to H_2S at each of two different distances $r = 2.33$ and 2.80 Å, the first of which corresponds to the $\text{S} \cdots \delta^+\text{H}$ distance in $\text{H}_2\text{S} \cdots \text{HF}$, are shown in Fig. 5 (see Fig. 3b for the corresponding definitions of r and φ). At both distances, two minima occur at ca. $\pm 85^\circ$, very similar to that (90°) expected of the n -pair model shown in Fig. 3b. It should be noted that the potential energy barrier is higher and the angle between the minima is much larger than is the case for H_2O (see Fig. 4), even when r is increased from 2.33 to 2.80 Å. The diagrams in Figs. 4 and 5 (and similar diagrams in [45]) demonstrate that the experimental observations about angular geometry and the rules deduced from them are consistent with an electrostatic model of the hydrogen bond. It is also of interest to note that although n -pairs are difficult to discern in the total electron densities of H_2S and H_2O , the electrostatic potentials around S and O show minima along those directions normally associated with n -pairs in the exaggerated models of Fig. 3.

The complexes $\text{H}_2\text{Z} \cdots \text{ICl}$ and $\text{H}_2\text{Z} \cdots \text{ICF}_3$ ($\text{Z} = \text{O}$ or S) can be examined in more detail in the light of the foregoing discussion of electronic models of H_2O and H_2S . It was shown by means of observations in the rotational spectra of both $\text{H}_2\text{O} \cdots \text{ICl}$ [5] and $\text{H}_2\text{O} \cdots \text{ICF}_3$ [14] that the H, O and I atoms must be effectively coplanar in the zero-point state, i.e. the potential energy as a function of the angle φ (see Table 1 for definition of φ) is either of the single minimum type with $\varphi = 0$ at the minimum or is of the double minimum type ($|\varphi_{\min}| > 0$) but with a barrier at

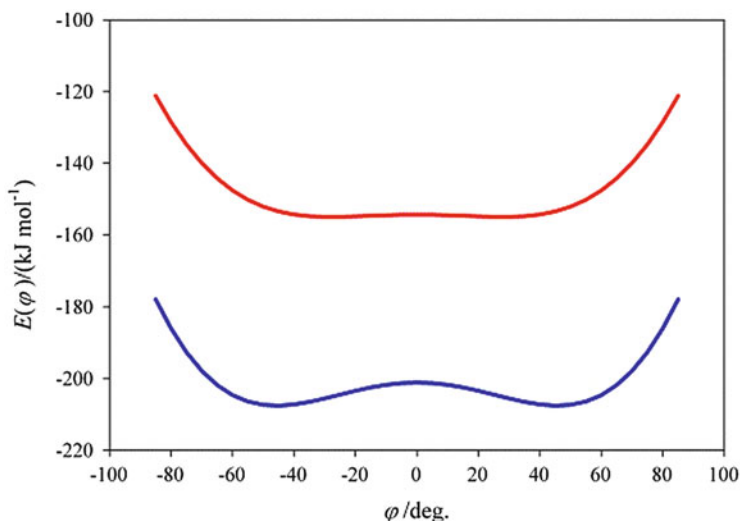


Fig. 4 The electrostatic potential $E(\varphi)$ near to the oxygen atom in H_2O as a function of the angle φ defined in Fig. 3a. The electrostatic potential is the potential energy of a non-perturbing unit positive charge at (r, φ) . The *upper curve* is generated by taking \oplus around the O atom in the plane containing the n -pair axes at the fixed distance $r = 1.5 \text{ \AA}$. The *lower curve* is obtained in a similar way at the distance $r = 1.75 \text{ \AA}$. See text for discussion

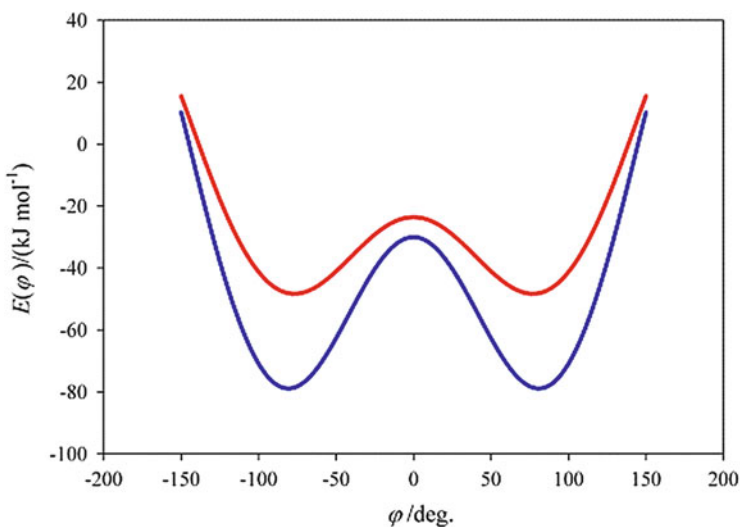


Fig. 5 The electrostatic potential $E(\varphi)$ close to the sulfur atom in H_2S as a function of the angle φ defined in Fig. 3b. The electrostatic potential is the potential energy of a non-perturbing unit positive charge at (r, φ) . The *upper curve* is generated by taking \oplus around the S atom in the plane containing the n -pair axes at the fixed distance $r = 2.33 \text{ \AA}$. The *lower curve* is obtained in a similar way at the distance $r = 2.80 \text{ \AA}$. See text for discussion

$\varphi = 0$ sufficiently low that inversion of the configuration at O is rapid on the microwave timescale. Thus, the ground-state vibrational wavefunction reflects the symmetry of the coplanar arrangement. On the other hand, interpretations of the rotational spectra of both $\text{H}_2\text{S} \cdots \text{ICl}$ [6] and $\text{H}_2\text{S} \cdots \text{ICF}_3$ [14] reveal that in these complexes the potential energy barrier to the coplanar arrangement of the H, S and I atoms is sufficiently high and wide that inversion of the configuration is slow on the microwave timescale and the configuration at S is therefore permanently pyramidal on that timescale. Similar contrasting results were found experimentally for $\text{H}_2\text{O} \cdots \text{HF}$ [49] and $\text{H}_2\text{S} \cdots \text{HF}$ [50, 51] and provide further evidence that the simple electrostatic n -pair model is appropriate for $\text{H}_2\text{Z} \cdots \text{ICl}$ and $\text{H}_2\text{Z} \cdots \text{ICF}_3$ ($\text{Z} = \text{O}$ or S). These semi-quantitative conclusions about the general forms of the potential energy functions $V(\varphi)$ available from the rotational spectra and from the simple electrostatic model were confirmed and made quantitative by means of ab initio calculations as follows.

The geometry of each $\text{H}_2\text{Z} \cdots \text{IR}$ ($\text{Z} = \text{O}$ or S ; $\text{R} = \text{Cl}$ or CF_3) was optimised at a fixed angle φ at the CCSD(T)(F12*)/cc-pVDZ-F12 level of theory to give the energy $V(\varphi)$ using the MOLPRO program [52]. A collinear arrangement $\text{Z} \cdots \text{I}-\text{R}$ of the halogen bond was assumed. The explicitly correlated (F12*) level of theory [53, 54] was the best compromise between accuracy and computational time available. For iodine, the cc-pVDZ-PP-F12 basis set, where PP indicates a pseudopotential replacing the 28 inner core electrons, was used [55]. The CF_3I and H_2Z molecules were assumed to retain their C_{3v} and C_{2v} symmetries, respectively, when subsumed into the complex. In the cases of $\text{H}_2\text{O} \cdots \text{ICF}_3$ and $\text{H}_2\text{S} \cdots \text{ICF}_3$ there is the additional degree of vibrational (torsional) freedom associated with the internal rotation of the H_2Z molecule with respect to the CF_3 group. In fact, the potential energy barrier to internal rotation is extremely small in these molecules. At the level of theory employed, the difference in energy (expressed as a wavenumber here) between the two limiting forms in which the $\text{Z}-\text{H}$ bonds are eclipsed and staggered with respect to the $\text{C}-\text{F}$ bonds is at most a few cm^{-1} , whatever the angle φ . In the calculations reported here, the energy obtained refers to the fixed angle φ with the $\text{C}-\text{F}$ and $\text{Z}-\text{H}$ bonds fully staggered. This procedure was repeated for a sufficient range of φ values to give $V(\varphi)$ as a function of φ . Corrections for basis set superposition error are small for basis functions optimised for F12 methods (for example, the BSSE corrections to the PE barrier heights of 115 and $1,175 \text{ cm}^{-1}$ in $\text{H}_2\text{O} \cdots \text{HF}$ and $\text{H}_2\text{S} \cdots \text{HF}$, respectively, corresponded to only 4 and 16 cm^{-1} (Legon and Tew (2014), unpublished observations)) and have not been applied here. Potential energy functions generated in this manner for various $\text{H}_2\text{O} \cdots \text{HX}$, $\text{H}_2\text{O} \cdots \text{XY}$, $\text{H}_2\text{S} \cdots \text{HX}$ and $\text{H}_2\text{S} \cdots \text{XY}$ complexes [49, 56–58] can be fitted (by the least-squares method) with reasonable accuracy to an analytical, double-minimum potential energy function of the type

$$V(\varphi) = \alpha\varphi^4 - \beta\varphi^2, \quad (9)$$

where α and β are positive constants. This type of function can be readily converted to the form

$$V(z) = a(z^4 - bz^2), \quad (10)$$

in which z is a dimensionless, reduced coordinate related to φ by means of the expression

$$\varphi = (r_H \cos \frac{1}{2}\theta)^{-1} (2\mu/\hbar^2)^{-\frac{1}{2}} a^{-\frac{1}{2}} z, \quad (11)$$

In Eq. (11), r_H is the Z–H distance, θ is the angle HZH and μ is the reduced mass for the inversion in question. When a curvilinear motion is assumed for the H atoms of H_2Z in $H_2Z \cdots IR$ ($R = Cl$ or CF_3), the definition of the reduced mass appropriate to the form $V(\varphi) = \alpha\varphi^4 - \beta\varphi^2$ is [49, 59]

$$\begin{aligned} \frac{1}{\mu} = & \frac{1}{M_{XY}} \left(\frac{r_H \cos \frac{1}{2}\theta}{r_{cm}} \right)^2 + \frac{1}{4M_H} + \frac{1}{4M_X} \\ & + \frac{1}{M_Z} \left\{ \left(\frac{r_H \cos \frac{1}{2}\theta}{r_{cm}} \right)^2 + \frac{2r_H \cos \frac{1}{2}\theta \cos \varphi}{r_{cm}} + 1 \right\}. \end{aligned} \quad (12)$$

The expressions that relate the coefficients α , β , a and b are

$$\alpha = (r_H \cos \frac{1}{2}\theta)^4 (2\mu/\hbar^2)^2 a^3, \quad (13)$$

and

$$\beta = (r_H \cos \frac{1}{2}\theta)^2 (2\mu/\hbar^2) a^2 b. \quad (14)$$

The energy levels associated with the one-dimensional motion described by the reduced coordinate z and governed by the potential energy expression Eq. (10) can be calculated by using the program *Anharm*.¹ These energy levels (expressed as wavenumbers) for $H_2O \cdots ICl$ and $H_2O \cdots ICF_3$ are shown together with the corresponding fitted functions $V(\varphi) = \alpha\varphi^4 - \beta\varphi^2$ in Fig. 6a, b, respectively, while the results for $H_2S \cdots ICl$ and $H_2S \cdots ICF_3$ are in Fig. 7a, b, respectively. We note that the functions and their associated energy levels confirm that both $H_2O \cdots ICl$ and $H_2O \cdots ICF_3$ have a sufficiently low potential energy barrier to the planar configuration at O to ensure that the molecules are effectively planar in the sense defined earlier. Indeed, the PE barrier in the case of $H_2O \cdots ICF_3$ is so close to zero ($< 2 \text{ cm}^{-1}$) that the $H_2O \cdots I-C$ group of atoms may be taken as planar. The frequency associated with the motion that inverts the configuration at O (or S) corresponds to the separation between the two lowest energy levels ($v=0$ and 1). The inversion frequency for both $H_2O \cdots ICl$ and $H_2O \cdots ICF_3$ is very much greater

¹ The program *Anharm* was originally developed by Johan Mj  berg (see [60]). The version used here is the one modified by Kisiel Z. <http://www.ifpan.edu.pl/~kisiel/prospe.htm>

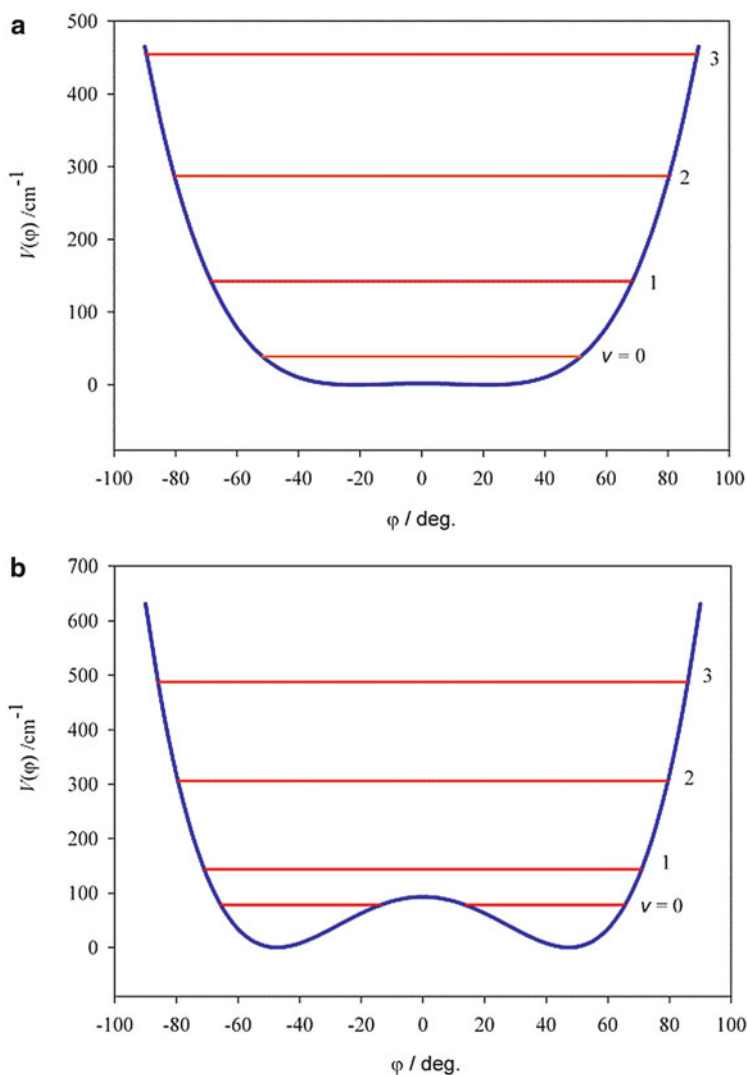


Fig. 6 The potential energy $V(\varphi)$ of the molecules (a) $\text{H}_2\text{O} \cdots \text{ICl}$ and (b) $\text{H}_2\text{O} \cdots \text{ICF}_3$ as a function of the angle φ made by the extension of the C_2 axis of the H_2O molecule with the $\text{O} \cdots \text{I}$ internuclear axis (as defined in Table 1). Each curve corresponds to a spline-function fit of the energies of the optimized geometry obtained at each of a series of angles φ , when varied in 5° steps from 0° to 100° . The geometry was optimized at the CCSD(T)(F12*)/cc-pVDZ-F12 level of theory at each angle. The method of obtaining the vibrational energy levels v associated with the potential energy curve is discussed in the text

than the (microwave) frequencies associated with rotational transitions and in that sense the molecule is planar on the microwave timescale but pyramidal at equilibrium. This conclusion holds for all halogen-bonded complexes $\text{H}_2\text{O} \cdots \text{XY}$ and all

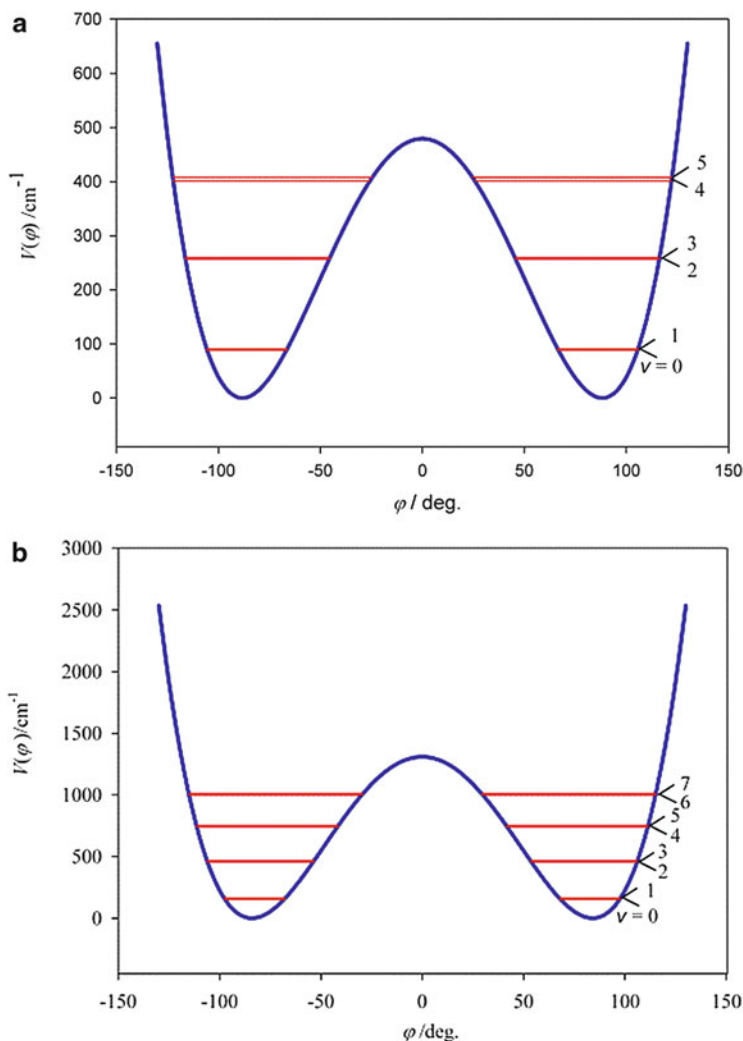


Fig. 7 The potential energy $V(\varphi)$ of the molecules (a) $\text{H}_2\text{S} \cdots \text{ICl}$ and (b) $\text{H}_2\text{S} \cdots \text{ICF}_3$ as a function of the angle φ made by the extension of the C_2 axis of the H_2S molecule with the $\text{S} \cdots \text{I}$ internuclear axis (as defined in Table 1). The method of obtaining the potential energy curve and its associated vibrational energy levels is as referred to in the legend for Fig. 6

hydrogen-bonded complexes $\text{H}_2\text{O} \cdots \text{HX}$ so far investigated and the potential energy functions for all $\text{H}_2\text{O} \cdots \text{HX}$ (Ligon AC, Tew DP (2014), unpublished observations) [49, 56–58] are similar to those for $\text{H}_2\text{O} \cdots \text{ICl}$ and $\text{H}_2\text{O} \cdots \text{ICF}_3$.

It is a well-known property of double minimum functions such as those discussed here that, as the associated energy levels drop below the top of the potential energy barrier, they draw together rapidly in pairs and in the limit of a high, wide barrier the members of each pair become degenerate. Both $\text{H}_2\text{S} \cdots \text{ICl}$

and $\text{H}_2\text{S} \cdots \text{ICF}_3$ have potential energy functions $V(\varphi)$ in which the barrier is sufficiently high and broad that the lower energy levels exhibit this effect (see Fig. 7a, b). In both cases, the separation between the lowest energy pair ($v=0$ and 1) corresponds to a frequency of less than a few kilohertz, i.e. very small on the microwave timescale. Clearly, both $\text{H}_2\text{S} \cdots \text{ICl}$ and $\text{H}_2\text{S} \cdots \text{ICF}_3$ have non-inverting pyramidal configurations at S. This difference in the height and width of the potential energy barrier at $\varphi=0$ between the H_2S and H_2O complexes can be understood in the light of the discussion of the electrostatic potential outside these molecules given earlier.

The near-degeneracy of the $v=0$ and 1 levels has been noted for all halogen-bonded complexes $\text{H}_2\text{S} \cdots \text{XY}$ and hydrogen-bonded complexes $\text{H}_2\text{S} \cdots \text{HX}$ investigated so far (Legon and Tew (2014), unpublished observations) and leads to consequences (e.g. absence of certain transitions) in the rotational spectra when observed at very low temperatures in supersonically expanded gas pulses. When identified, such consequences allow the conclusion that these molecules are pyramidal at S.

4.2 Radial Geometry: How Do the Halogen Bond Distances $\text{Z} \cdots \text{I}$ Vary from $\text{B} \cdots \text{ICl}$ to $\text{B} \cdots \text{ICF}_3$?

Table 2 compares the distances $r(\text{Z} \cdots \text{I})$ in $\text{B} \cdots \text{ICl}$ and $\text{B} \cdots \text{ICF}_3$ obtained through interpretation of spectroscopic constants (see Sect. 3.1) with those calculated ab initio at the CCSD(T)(F12*)/cc-pVDZ-F12 level of theory, where Z is either the halogen bond acceptor atom or centre (in those cases where B is a π electron donor). In the geometry optimisations, collinear $\text{Z} \cdots \text{I} \cdots \text{C}$ and $\text{Z} \cdots \text{I} \cdots \text{Cl}$ nuclei were assumed for $\text{B} = \text{H}_2\text{O}$ and H_2S , i.e. in those complexes for which these systems were not constrained by symmetry to be collinear. In the complexes $\text{C}_2\text{H}_2 \cdots \text{IR}$ and $\text{C}_2\text{H}_4 \cdots \text{IR}$, small angular distortions ($<1^\circ$) resulting from a symmetrical movement of the H atoms away from the line of the two C atoms were detected.

Also recorded in Table 2 are the experimental and calculated differences $\Delta r(\text{Z} \cdots \text{I})$ in the length of the halogen bonds of $\text{B} \cdots \text{ICF}_3$ and $\text{B} \cdots \text{ICl}$. It is known (see Section 3.1) that the experimental distances are of the r_0 variety, while those from the ab initio calculations are r_e values. We note several points in connection with Table 2. First, the distances $r(\text{Z} \cdots \text{I})$ are well predicted by the ab initio calculations for the complexes $\text{B} \cdots \text{ICl}$, with the exception of $\text{B} = \text{NH}_3$ for which the experimental value is ~ 0.1 Å longer than that calculated. The complex $\text{H}_3\text{N} \cdots \text{ICF}_3$ is, however, well-behaved in this respect. Of relevance here is the distance $r_e(\text{N} \cdots \text{I}) = 2.605$ Å obtained from a geometry optimisation of $\text{H}_3\text{N} \cdots \text{ICl}$ conducted at the counterpoise corrected, CCSD(T)(F12b)/VTZ level of theory [61]. This differs by

Table 2 Observed and calculated intermolecular bond lengths $r(\text{Z} \cdots \text{I})$ in complexes $\text{B} \cdots \text{ICF}_3$ and $\text{B} \cdots \text{ICl}$

Lewis base B	$r_0(\text{Z} \cdots \text{I})/\text{\AA}$ from experiment			$r_e(\text{Z} \cdots \text{I})/\text{\AA}$ calculated ab initio ^a			$\sigma(\text{Z}) + \sigma(\text{I})/\text{\AA}^b$
	$\text{B} \cdots \text{ICF}_3$	$\text{B} \cdots \text{ICl}$	Δr	$\text{B} \cdots \text{ICF}_3$	$\text{B} \cdots \text{ICl}$	Δr	
N_2	3.441(1) ^c	3.180(2) ^d	0.258(3)	3.467	3.187	0.280	3.53
OC	3.428(1) ^e	3.011(1) ^f	0.417(2)	3.456	3.003	0.453	3.68
HCN	...	2.850(1) ^g	...	3.168	2.840	0.328	3.53
C_2H_4	3.434(2) ^h	3.032(2) ⁱ	0.402(4)	3.428	2.959	0.469	3.68
C_2H_2	3.442(2) ^j	3.115(2) ^k	0.327(4)	3.453	3.090	0.363	3.68
H_2O	3.053(2) ^l	2.828(1) ^m	0.225(3)	3.044	2.776	0.268	3.50
H_2S	3.559(1) ^l	3.154(3) ⁿ	0.405(4)	3.559	3.120	0.439	3.78
H_3P	3.571(3) ^o	2.963(1) ^p	0.608(4)	3.597	2.898	0.699	3.78
H_3N	3.038(1) ^q	2.711(2) ^r	0.327(3)	2.991	2.599	0.392	3.53

^aCalculations at the CCSD(T)(F12*)/cc-pVDZ-F12 level of theory^bFrom [62], ^c[10], ^d[1], ^e[11], ^f[2], ^g[7], ^h[13], ⁱ[4], ^j[12], ^k[3], ^l[14], ^m[5]. The value 2.838 Å quoted in [5] is a misprint. ⁿ[6], ^o[16], ^p[9], ^q[15], ^r[8]

only 0.006 Å from the value reported in Table 2. Mostly, the r_0 quantities are slightly longer than the calculated r_e values but not always. For diatomic molecules, it is known that $r_0 > r_e$ and this order is expected for normal polyatomic molecules. Second, the $\text{Z} \cdots \text{I}$ bond is systematically longer in $\text{B} \cdots \text{ICF}_3$ than in $\text{B} \cdots \text{ICl}$ complexes, a result consistent with the finding reported in Sect. 4.3 that, for a given B, the intermolecular bond is stronger in $\text{B} \cdots \text{ICl}$ complexes than in their $\text{B} \cdots \text{ICF}_3$ analogues, as measured by the intermolecular stretching force constant k_σ . The ab initio values of Δr are always larger than the experimental quantities. In both $\text{B} \cdots \text{ICl}$ and $\text{B} \cdots \text{ICF}_3$ the distances $r(\text{Z} \cdots \text{I})$ are significantly shorter than the sums of the van der Waals radii $\sigma(\text{Z})$ and $\sigma(\text{I})$ [62] of the atoms Z and I, which are also given in Table 2. This is readily understood in terms of the σ -hole concept for the halogen bond (see Sect. 4.3) introduced by Politzer et al. [63]. The σ -hole is closely related to the reduced van der Waals radius along the bond in Cl_2 , for example, relative to that perpendicular to it, as discussed by Stone [64] and others [65], and to the known sign of the molecular electric quadrupole moment of Cl_2 .

4.3 Intermolecular Stretching Force Constants k_σ : How Does Replacement of Cl in $\text{B} \cdots \text{ICl}$ by CF_3 Change the Electrophilicity of the Halogen Bond Donor Molecule?

The measure of the binding strength of $\text{B} \cdots \text{ICF}_3$ and $\text{B} \cdots \text{ICl}$ complexes in the gas phase that is most commonly available experimentally is the intermolecular

stretching force constant k_σ , the method for the determination of which from centrifugal distortion constants was set out in Sect. 3.2. Values of k_σ obtained in this way for both series are set out in Table 3.

It is clear from Table 3 that complexes $B \cdots ICl$ are systematically stronger than the corresponding complexes $B \cdots ICF_3$ according to the k_σ criterion (i.e. the restoring force required for infinitesimal increase of the intermolecular bond length $Z \cdots I$), with the ratio $k_\sigma(B \cdots ICl)/k_\sigma(B \cdots ICF_3)$ of the order 2 or 3.

It has been shown [66] that the intermolecular stretching force constant k_σ for hydrogen-bonded complexes $B \cdots HX$ ($X=F, Cl, Br, I$ or CN) can be reproduced with reasonable accuracy by means of the expression

$$k_\sigma = cN_B E_{HX}, \quad (15)$$

in which N_B is a numerical nucleophilicity assigned to the Lewis base B , E_{HX} is a numerical electrophilicity of the acid HX and $c = 0.25 \text{ N m}^{-1}$ is a constant. A similar expression (but with E_{HX} replaced by E_{XY}) also holds for the halogen-bonded complexes $B \cdots XY$ ($XY = F_2, ClF, Cl_2, BrCl, Br_2$ or ICl). Figure 8 shows the value of k_σ plotted against N_B for the six series $B \cdots F_2$, $B \cdots ClF$, $B \cdots Cl_2$, $B \cdots BrCl$, $B \cdots Br_2$ and $B \cdots ICl$ [18, 28] for a range of simple Lewis bases B . The scale of N_B was defined by setting $E_{ICl} = 10.0$ and requiring that all points for the $B \cdots ICl$ plot lie on a perfectly straight line $k_\sigma = cN_B E_{ICl}$. The other five series of k_σ values are seen to lie on reasonably straight lines which pass through the origin when plotted against the N_B values so defined, although the points $B = NH_3$ are less well-behaved, probably because of significant polarization of charge on complex formation. The slopes of the lines in Fig. 8 are proportional to E_{XY} and indicate that the order of electrophilicity of the dihalogen molecules is

Table 3 Experimental values of k_σ intermolecular stretching force constants for the series $B \cdots ICl$ and $B \cdots ICF_3$; a measure of binding strength

B	$k_\sigma/(\text{N m}^{-1})^a$		$D_e/(\text{kJ mol}^{-1})^b$	
	$B \cdots ICF_3$	$B \cdots ICl$	$B \cdots ICF_3$	$B \cdots ICl$
N_2	2.954(1) ^c	5.35(2) ^d	4.2	7.1
OC	3.950(2) ^e	7.96(3) ^f	6.2	12.7
HCN	...	14.5(1) ^g	13.9	23.7
C_2H_4	4.95(1) ^h	14.0(1) ⁱ	10.2	21.5
C_2H_2	4.96(7) ^j	12.1(1) ^k	9.2	17.2
H_2O	8.8(1) ^l	15.9(2) ^m	14.9	24.7
H_2S	6.7(1) ^l	16.55(5) ⁿ	10.5	22.6
H_3P	6.27(2) ^o	20.7(1) ^p	10.4	28.9
H_3N	11.6(2) ^q	30.4(3) ^r	22.5	46.8

^aCalculated from centrifugal distortion constant D_J or Δ_J using the appropriate expression given in Sect. 3.2. Errors reflect only the experimental error in the centrifugal distortion constants

^bCalculated at the CCSDT(T)(F12*)/cc-pVDZ-F12 level of theory and corrected for BSSE. See also [67] for D_e values for the complexes $B \cdots ICl$, ^c[10], ^d[1], ^e[11], ^f[2], ^g[7], ^h[13], ⁱ[4], ^j[12], ^k[3], ^l[14], ^m[5], ⁿ[6], ^o[16], ^p[9], ^q[15], ^r[8]

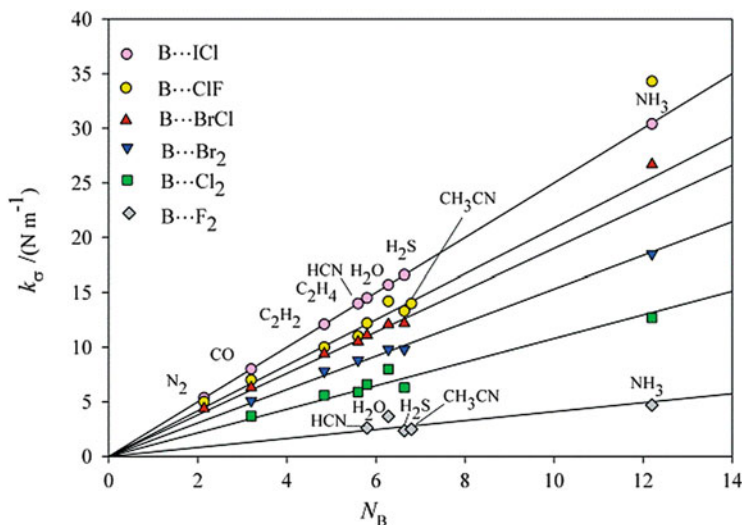
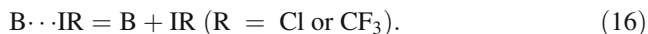


Fig. 8 The intermolecular force constant k_σ plotted against the nucleophilicity N_B of the Lewis base B for six series of halogen-bonded complexes $B \cdots XY$ ($XY = F_2, ClF, Cl_2, BrCl, Br_2$ or ICl). The values of N_B were defined by arranging the k_σ of the series $B \cdots ICl$ to lie on a straight line. The slope of each line yields the electrophilicity E_{XY} by means of Eq. (15) and the value $c = 0.25 \text{ N m}^{-1}$

$F_2 < Cl_2 < Br_2 < BrCl \sim ClF < ICl$. This order is in agreement with chemical intuition. The non-dipolar dihalogens have the smaller electrophilicities and these are in the order of their molecular electric quadrupole moments. The three polar species are more electrophilic. The question that now arises is whether Eq. (15) applies to $B \cdots ICF_3$ complexes and, if so, how does the electrophilicity of ICF_3 as a halogen bond donor compare with those of the dihalogen molecules in general and ICl in particular?

Figure 9 again shows k_σ plotted against N_B for the series $B \cdots ICl$, with $E_{ICl} = 10.0$ and the N_B values as defined in connection with Fig. 8. Also shown in Fig. 9 is the corresponding plot for the series $B \cdots ICF_3$. It is a reasonably straight line, with a slope which is about three times smaller than that for ICl but similar to that for the $B \cdots Cl_2$ series shown in Fig. 8. Evidently, the CF_3 group is less electron-withdrawing than Cl when bound to I and reduces the halogen bond donor ability of I to make it similar to that of Cl in Cl_2 .

Another measure of binding strength is the equilibrium dissociation energy D_e for the process



Values of D_e calculated at the explicitly correlated level of theory CCSD(T)(F12*)/cc-pVDZ-F12 are included in Table 3 for all $B \cdots ICF_3$ and $B \cdots ICl$. The calculations for the $B \cdots ICl$ series were carried out in connection with a detailed analysis of

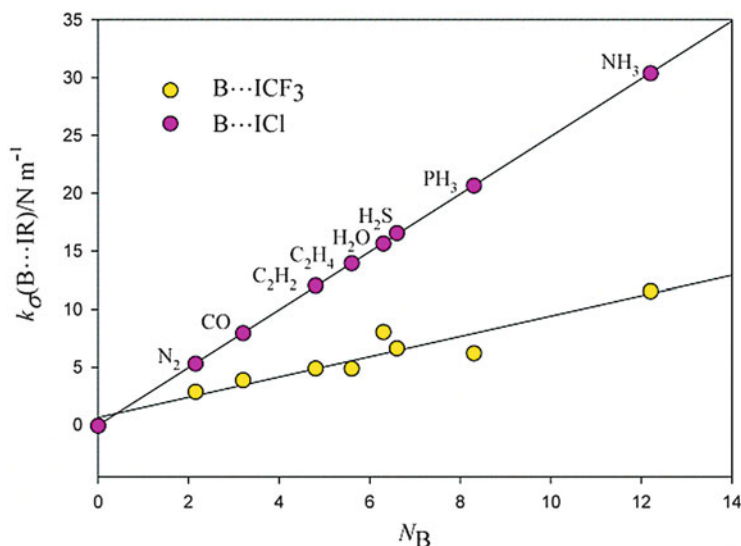


Fig. 9 k_σ plotted against N_B for the two series $B \cdots \text{ICl}$ and $B \cdots \text{ICF}_3$. The values of N_B were defined by arranging for the k_σ of the series $B \cdots \text{ICl}$ to lie on a straight line

D_e values for many $B \cdots \text{XY}$ and $B \cdots \text{HX}$ [67]. Corrections for basis set superposition error, although much reduced for F12-optimised basis functions, have been applied by using the Boys–Bernardi method [68]. The values of D_e shown in Table 3 for $\text{C}_2\text{H}_2 \cdots \text{ICF}_3$ and $\text{C}_2\text{H}_4 \cdots \text{ICF}_3$ are similar to those implied by measurement of ΔH for the process in liquid argon solution by Herrebout et al. and also D_e calculated by them at the MP2/aug-cc-pVTZ level of theory [69, 70]. Recent calculations at the MP2/DZVP level for $\text{H}_3\text{N} \cdots \text{ICF}_3$ and at the CCSDT(F12b)/VTZ-F12 level for $\text{H}_3\text{N} \cdots \text{ICl}$ yield $D_e = 24.3$ [71] and 54.0 kJ mol^{-1} [61], respectively. In general, the D_e values presented in Table 3 confirm the conclusion based on k_σ values, namely that, for a given B, the complex $B \cdots \text{ICF}_3$ is more weakly bound than the $B \cdots \text{ICl}$ complex. Moreover, k_σ and D_e appear to be proportional, as noted for the $\text{H}_3\text{N} \cdots \text{XY}$ series discussed in ref. [61] and established for a wide range of $B \cdots \text{XY}$ and $B \cdots \text{HX}$ in ref. [67].

This conclusion, based on two measures of binding strength (k_σ and D_e), is consistent with the σ -hole concept introduced by Politzer and co-workers [63]. The σ -hole is the positive region of molecular electrostatic surface potential (MESP) that occurs at I on the symmetry axes of ICl and ICF_3 , as displayed in Fig. 10. The σ -holes are evident as the red spots. The axial MESP for ICl is larger, more positive than that of ICF_3 , a result consistent with the greater electrophilicity of ICl than ICF_3 and the greater values of k_σ and D_e for a given B in the $B \cdots \text{ICl}$ series.

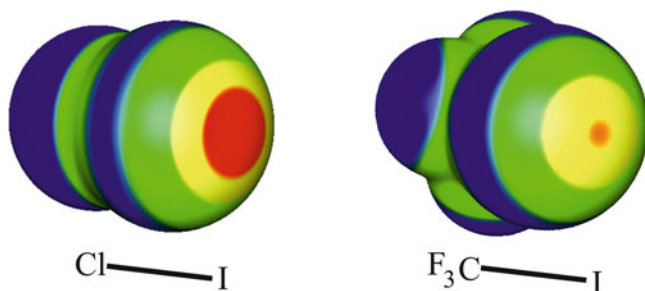


Fig. 10 The molecular electrostatic surface potentials (MESP) of ICl and ICF₃. Electrostatic potentials were computed on the 0.001 electron bohr⁻³ molecular surfaces using M06-2X/6-311G* optimisations for each molecule (see [63] for method of calculation). Colour ranges, in kJ mol⁻¹, are: red > 125, 125 > yellow > 63, 63 > green > 0 and blue < 0 (negative). The most positive MESPs are along the extensions of the Cl-I and C-I bonds and are 192 and 133 kJ mol⁻¹ for ICl and ICF₃, respectively. This diagram was kindly provided by Jane Murray and Peter Politzer

4.4 Electric Charge Rearrangement on Formation of B ··· ICl and B ··· ICF₃ Complexes

It was shown in Sect. 3.3 that the I and Cl nuclear quadrupole coupling constants χ_{zz}^e (I) and χ_{zz}^e (Cl) (defined in Eqs.(5) and (6)) of the ICl subunit within the complex B ··· ICl can be used in Eqs. (7) and (8) together with the free atom coupling constants χ_A (I) and χ_A (Cl) and the free ICl molecule constants χ_0 (I) and χ_0 (Cl) to obtain an estimate of δ_i , the fraction of an electronic charge that is transferred from the acceptor atom/centre Z of the Lewis base B to I. It was also indicated that Eqs.(7) and (8) must be corrected for the zero-point oscillations of the ICl subunit when within the complex if the zero-point (observed) coupling constants χ_{zz}^0 (I) and χ_{zz}^0 (Cl) are to be related to their equilibrium counterparts. The values of δ_i that result [9] for the series B ··· ICl, where B = N₂, CO, H₂O, C₂H₂, C₂H₄, H₂S, PH₃ and NH₃, when this procedure is applied are shown in Fig. 11. The values on the abscissa are the first ionization energies, I_B , of the Lewis bases; these were used to order the δ_i values because I_B provides a measure of the ease with which the highest energy electron may be removed from B. Also shown in Fig. 11 is the corresponding curve for the series B ··· Cl₂.

The important points about the curves in Fig. 11 are that the value of δ_i increases reasonably smoothly as B becomes easier to ionize (and presumably more polarizable) and that the curve for B ··· Cl₂ is much shallower than that of B ··· ICl (as might be expected from the more polar nature of ICl). Indeed, the value of δ_i is effectively zero for all but H₃N ··· Cl₂ and H₃P ··· Cl₂.

Unfortunately, this approach is not possible for the B ··· ICF₃ complexes because ICF₃ does not possess a second quadrupolar nucleus, as required by Eq. (8). Then only the difference ($\delta_i - \delta_p$) can be obtained from Eq. (7). Since δ_p is unknown, δ_i is

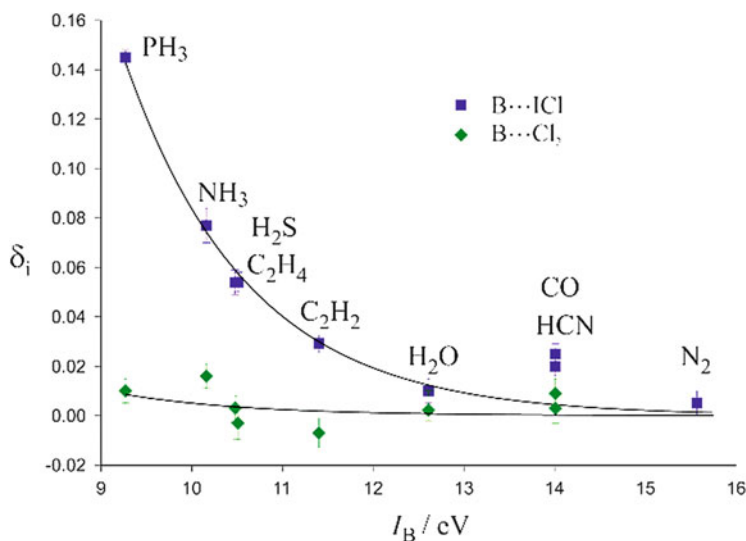


Fig. 11 The fraction δ_i of an electronic charge transferred from B to XY on formation of $B \cdots XY$ from B and XY plotted against the first ionization energy I_B of the Lewis base B for the two series of halogen-bonded complexes $B \cdots \text{ICl}$ and $B \cdots \text{Cl}_2$. δ_i was determined, by the method described in Sect. 3.3, from the changes in X and Y nuclear quadrupole coupling constants when XY is subsumed into the complex

unavailable. Some progress is possible, however, when we note that the strength of the intermolecular binding is considerably less in $B \cdots \text{ICF}_3$ than in the corresponding $B \cdots \text{ICl}$. In fact, a comparison of Figs. 8 and 9 reveals that the binding strength for $B \cdots \text{ICF}_3$ (as measured by k_σ) is similar to that of $B \cdots \text{Cl}_2$ for a given B or, put another way, $E_{\text{ICF}_3} \approx E_{\text{Cl}_2}$. Moreover, the distance of the atom I from the acceptor atom Z of B is always considerably greater in $B \cdots \text{ICF}_3$ than in $B \cdots \text{ICl}$ for a given B (see Table 2). Both of these observations suggest that the values of δ_i for the $B \cdots \text{ICF}_3$ series are much reduced from those of the $B \cdots \text{ICl}$ and are probably negligibly small, as they are for the $B \cdots \text{Cl}_2$.

Conclusions

This chapter first describes how to observe the rotational spectra of pairs of molecules held together by a weak intermolecular bond, as exemplified by the halogen bonds in the series of complexes $B \cdots \text{ICl}$ and $B \cdots \text{ICF}_3$. The various properties of such complexes in the gas phase that can be determined from their rotational spectra under various levels of approximation are next discussed. A comparison of the angular geometries, radial geometries and strength of the intermolecular bond, the last of these as defined by the intermolecular force constants k_σ , reveals several similarities between the

(continued)

two series of complexes. It is shown that the complexes $B \cdots ICF_3$ also obey a set of rules originally enunciated to rationalise the angular geometries of hydrogen-bonded complexes of the type $B \cdots HX$, but which were subsequently found to apply to their halogen-bonded analogues $B \cdots XY$, where XY is a dihalogen molecule such as ICl . Important in establishing the validity of these rules in the case of the $B \cdots ICF_3$ series are the complexes in which $B = H_2O$ and H_2S . These exhibit out-of-plane angles φ which differ markedly from $B = H_2O$ to $B = H_2S$. Thus, H_2O forms a complex $H_2O \cdots ICF_3$ in which the configuration at O is either planar or effectively planar, i.e. rapidly inverting between equivalent pyramidal arrangements. On the other hand, the configuration at S in $H_2S \cdots ICF_3$ is permanently pyramidal. This contrast is also found for the pair $H_2O \cdots ICl$ and $H_2S \cdots ICl$. Ab initio calculations performed at the CCSD(T)(F12*)/cc-pVDZ-F12 level of theory generated potential energy functions governing the inversion of configuration at O or S. For both $H_2O \cdots ICF_3$ and $H_2O \cdots ICl$ each function has a low barrier to the planar arrangement but the barriers are much higher and wider in the corresponding H_2S complexes. In the lowest states, the rates of inversion are high compared with the timescale of molecular rotations for the two H_2O complexes but are negligible for the H_2S pair.

The values of the intermolecular stretching force constants k_σ for the two series $B \cdots ICF_3$ and $B \cdots ICl$ show that the former series is systematically more weakly bound than the latter. Interpretation of k_σ values in terms of a nucleophilicity N_B assigned to the Lewis bases B and an electrophilicity E_{IR} assigned to the Lewis acids/halogen bond donors $IR = ICl$ and ICF_3 reveals that replacement of the chlorine atom in ICl by a CF_3 group leads to an E_{ICF_3} value which is approximately $E_{ICl}/3$ and which is similar to that of Cl_2 . Finally, it is argued that amount of electronic charge redistributed from B to ICF_3 on formation of $B \cdots ICF_3$ is probably negligibly small.

Acknowledgements Support by the EPSRC of various aspects of the work reported here is gratefully acknowledged (NRW for Grant No. EP/G026424/1 and ACL for a Senior Fellowship). We are also pleased to acknowledge a Senior Research Fellowship of the University of Bristol, a Leverhulme Emeritus Fellowship (ACL) and Royal Society University Research Fellowships (DPT and NRW). We also thank Jane Murray and Peter Politzer for providing Fig. 10.

References

1. Davey JB, Legon AC, Wacławik ER (2000) Measurement of inter- and intramolecular charge transfer in the complex $N_2 \cdots ICl$ from analysis of halogen nuclear quadrupole hyperfine structure in the rotational spectrum. *J Mol Struct* 500:391–402

2. Davey JB, Legon AC, Waclawik ER (1999) Inter- and intra-molecular electron transfer in the complex $\text{OC} \cdots \text{ICl}$ determined from iodine and chlorine nuclear quadrupole hyperfine structure in its rotational spectrum. *Phys Chem Chem Phys* 1:3097–3102
3. Davey JB, Legon AC (1999) Rotational spectroscopy of mixtures of ethyne and iodine monochloride: isolation and characterisation of the π -type complex $\text{C}_2\text{H}_2 \cdots \text{ICl}$. *Phys Chem Chem Phys* 1:3721–3726
4. Thumwood JMA, Legon AC (1999) A π -electron donor-acceptor complex of ethene and iodine monochloride: geometry, binding strength and charge redistribution determined by rotational spectroscopy. *Chem Phys Letts* 310:88–96
5. Davey JB, Legon AC, Waclawik ER (2000) An investigation of the gas-phase complex of water and iodine monochloride by microwave spectroscopy: geometry, binding strength and electron redistribution. *Phys Chem Chem Phys* 2:1659–1665
6. Legon AC, Waclawik ER (1999) Angular geometry, binding strength and charge transfer for the complex $\text{H}_2\text{S} \cdots \text{ICl}$ determined by rotational spectroscopy. *Chem Phys Letts* 312:385–393
7. Herrebout WA, Legon AC, Waclawik ER (1999) Is there a significant intermolecular charge transfer in the ground state of the $\text{HCN} \cdots \text{ICl}$ complex? An answer from rotational spectroscopy. *Phys Chem Chem Phys* 1:4961–4966
8. Waclawik ER, Legon AC (1999) Halogen nuclear quadrupole coupling in the rotational spectrum of $\text{H}_3\text{N} \cdots \text{ICl}$ as a probe of inter- and intramolecular transfer. *Phys Chem Chem Phys* 1:4695–4700
9. Davey JB, Legon AC, Waclawik ER (2000) Inter- and intramolecular electronic transfer on formation of $\text{H}_3\text{P} \cdots \text{ICl}$ as determined by rotational spectroscopy. *Phys Chem Chem Phys* 2:2265–2269
10. Anable JP, Hird DE, Stephens SL, Zaleski DP, Walker NR, Legon AC (2014) The rotational spectrum of $\text{N}_2 \cdots \text{ICF}_3$ observed with a broadband, chirped-pulse FT microwave spectrometer. Manuscript in preparation
11. Stephens SL, Walker NR, Legon AC (2011) Rotational spectra and properties of complexes $\text{B} \cdots \text{ICF}_3$ ($\text{B} = \text{Kr}$ or CO) and a comparison of the efficacy of ICl and ICF_3 as iodine donors in halogen bond formation. *J Chem Phys* 135:224309
12. Stephens SL, Walker NR, Legon AC (2014) Broadband rotational spectroscopy of the ethyne $\cdots \text{ICF}_3$ complex in the microwave region. Manuscript in preparation
13. Stephens SL, Mizukami W, Tew DP, Walker NR, Legon AC (2012) The halogen bond between ethene and a simple perfluoroiodoalkane: $\text{C}_2\text{H}_4 \cdots \text{ICF}_3$ identified by broadband rotational spectroscopy. *J Mol Spectrosc* 280:47–53
14. Stephens SL, Walker NR, Legon AC (2011) Molecular geometries of $\text{H}_2\text{S} \cdots \text{ICF}_3$ and $\text{H}_2\text{O} \cdots \text{ICF}_3$ characterised by broadband rotational spectroscopy. *Phys Chem Chem Phys* 13:21093–21101
15. Stephens SL, Walker NR, Legon AC (2011) Internal rotation and halogen bonds in $\text{CF}_3\text{I} \cdots \text{NH}_3$ and $\text{CF}_3\text{I} \cdots \text{N}(\text{CH}_3)_3$ probed by broadband rotational spectroscopy. *Phys Chem Chem Phys* 13:20736–20744
16. Stephens SL, Walker NR, Legon AC (2014) The broadband rotational spectrum of $\text{H}_3\text{P} \cdots \text{ICF}_3$ and internal rotation. Manuscript in preparation
17. Legon AC (1998) π -Electron ‘donor-acceptor’ complexes $\text{B} \cdots \text{ClF}$ and the existence of the ‘chlorine’ bond. *Chem Eur J* 4:1890–1897
18. Legon AC (1999) Pre-reactive complexes of dihalogens XY with Lewis bases B in the gas phase: a systematic case for the ‘halogen’ analogue $\text{B} \cdots \text{XY}$ of the hydrogen bond $\text{B} \cdots \text{HX}$. *Angew Chem Int Ed Engl* 38:2686–2714
19. Legon AC (2008) The interaction of dihalogens and hydrogen halides with Lewis bases in the gas phase: an experimental comparison of the halogen bond and the hydrogen bond. In: Metrangola P, Resnati G (eds) *Halogen bonding: fundamentals and applications. Structure and bonding*, vol 126. Springer, Berlin, pp 17–64
20. Legon AC (2010) The halogen bond: an interim perspective. *Phys Chem Chem Phys* 12:7736–7747

21. Evangelisti L, Feng G, Eciija P, Cocinero EJ, Fernando Castaño F, Caminati WA (2011) The halogen bond and internal dynamics in the molecular complex of CF_3Cl and H_2O . *Angew Chem Int Ed Engl* 50:7807–7810
22. Feng G, Evangelisti L, Gasparini N, Caminati W (2012) On the $\text{Cl} \cdots \text{N}$ halogen bond: a rotational study of $\text{CF}_3\text{Cl} \cdots \text{NH}_3$. *Chem Eur J* 18:1364–1368
23. Evangelisti L, Feng G, Gou Q, Guidetti G, Caminati W (2012) Orientation of the water moiety in $\text{CF}_4\text{-H}_2\text{O}$. *J Mol Spectrosc* 282:39–41
24. Springer SD, Rivera-Rivera LA, Scott KW, McElmurry BA, Wang Z, Leonov II, Lucchese RR, Legon AC, Bevan JW (2012) A CMM-RS potential for characterization of the properties of the halogen-bonded OC-Cl_2 complex. *J Phys Chem A* 116:1213–1223
25. Legon AC (1995) Mulliken $n.\text{a}\sigma^*$ and $b\pi.\text{a}\sigma^*$ complexes $\text{B} \cdots \text{Cl}_2$ in the gas phase: rules for predicting angular geometries and nature of the interaction. *Chem Phys Lett* 237:291–298
26. Legon AC (1995) Donor-acceptor complexes of Lewis bases with bromine monochloride in the gas phase: some generalisations from rotational spectroscopy. *J Chem Soc Faraday Trans* 91:1881–1883
27. Legon AC (1997) Nature of complexes $\text{B} \cdots \text{ClF}$ in the gas phase: conclusions from systematic variation of the Lewis base B and a comparison of the $\text{B} \cdots \text{ClF/B} \cdots \text{HCl}$ series. *Chem Phys Lett* 279:55–64
28. Legon AC (1998) Quantitative gas-phase electrophilicities of the dihalogen molecules $\text{XY}=\text{F}_2, \text{Cl}_2, \text{Br}_2, \text{BrCl}$ and ClF . *J Chem Soc Chem Commun* 2585–2586
29. Legon AC (1999) Angular and radial geometries, charge transfer and binding strength in isolated complexes $\text{B} \cdots \text{ICl}$: some generalisations. *Chem Phys Lett* 314:472–480
30. Legon AC (1998) The nature of the interaction of molecular fluorine and Lewis bases B from a comparison of the properties of $\text{B} \cdots \text{F}_2$ and $\text{B} \cdots \text{HF}$. *J Chem Soc Chem Commun* 2737–2738
31. Stone AJ (2013) Are halogen bonds electrostatically driven? *J Am Chem Soc* 135:7005–7009
32. Metrangolo P, Meyer F, Pilati T, Resnati G, Terraneo G (2008) Halogen bonding in supramolecular chemistry. *Angew Chem Int Ed Engl* 47:6114–6127
33. Balle TJ, Flygare WH (1981) Fabry-Perot cavity Fourier transform microwave spectroscopy with a pulsed nozzle particle source. *Rev Sci Instrum* 52:33–45
34. Legon AC (1992) Fourier transform microwave spectroscopy. In: Scoles G (ed) *Atomic and molecular beam methods*, vol 2. Oxford University Press, New York, pp 289–308
35. Brown GG, Dian BC, Douglass KO, Geyer SM, Shipman SS, Pate BH (2008) A broadband Fourier transform microwave spectrometer based on chirped pulse excitation. *Rev Sci Instrum* 79:053103-1-13
36. Stephens SL, Walker NR (2010) Determination of nuclear spin-rotation coupling constants in CF_3I by chirped-pulse Fourier-transform microwave spectroscopy. *J Mol Spectrosc* 263:27–33
37. Kraitchman J (1953) Determination of molecular structures from microwave spectroscopic data. *Am J Phys* 21:17–24
38. Costain CC (1958) Determination of molecular structure from ground-state spectroscopic constants. *J Chem Phys* 29:864–874
39. Gordy W, Cook RL (1984) Microwave molecular spectra. In: Weissberger A (ed) *Techniques of chemistry*, vol 56. Wiley, New York, pp 726–795
40. Herzberg G (1950) Molecular spectra and molecular structure. I. Spectra of diatomic molecules, 2nd edn. Van Nostrand, New York, p 103
41. Millen DJ (1985) Determination of stretching force constants of weakly bound dimers from centrifugal distortion constants. *Can J Chem* 63:1477–1479
42. Townes CH, Schawlow AL (1955) *Microwave spectroscopy*. McGraw-Hill, New York, Chap 9, p 225
43. Legon AC, Millen DJ (1982) Determination of properties of hydrogen-bonded dimers by rotational spectroscopy and a classification of dimer geometries. *Faraday Discuss Chem Soc* 73:71–87
44. Legon AC, Millen DJ (1987) Directional character, strength and nature of the hydrogen bond in gas-phase dimers. *Acc Chem Res* 20:39–46

45. Legon AC, Millen DJ (1987) Angular geometries and other properties of hydrogen-bonded dimers: a simple electrostatic interpretation based on the success of the electron-pair model. *Chem Soc Rev* 16:467–498
46. Stone AJ (1981) Distributed multipole analysis or how to describe molecular charge distributions. *Chem Phys Lett* 83:233–239
47. Buckingham AD, Fowler PW (1985) A model for the geometries of van der Waals complexes. *Can J Chem* 63:2018–2025
48. Buckingham AD (1967) Permanent and induced molecular moments and long-range intermolecular forces. *Adv Chem Phys* 12:107–142
49. Kisiel Z, Legon AC, Millen DJ (1982) Spectroscopic investigations of hydrogen bonding interactions in the gas phase. VII. The equilibrium conformation and out-of-plane bending potential energy function of the hydrogen-bonded heterodimer $\text{H}_2\text{O} \cdots \text{HF}$ determined from its microwave rotational spectrum. *Proc R Soc Lond A* 381:419–442
50. Viswanathan R, Dyke TR (1982) The structure of $\text{H}_2\text{S} \cdots \text{HF}$ and the stereochemistry of the hydrogen bond. *J Chem Phys* 77:1166–1174
51. Willoughby LC, Fillery-Travis AJ, Legon AC (1984) An investigation of the rotational spectrum of $\text{H}_2\text{S} \cdots \text{HF}$ by pulsed-nozzle, Fourier-transform microwave spectroscopy: determination of the hyperfine coupling constants $\chi_{aa}({}^{33}\text{S})$, χ_{aa}^{D} and $D_{aa}^{\text{H(D)F}}$. *J Chem Phys* 81:20–26
52. Werner HJ, Knowles PJ, Knizia G, Manby FR, Schütz M et al (2012) MOLPRO, version 2012.1, a package of ab initio programs. <http://www.molpro.net>
53. Hättig C, Tew DP, Köhn A (2010) Accurate and efficient approximations to explicitly correlated coupled-cluster singles and doubles, CCSD-F12. *J Chem Phys* 132:231102
54. Peterson KA, Adler TB, Werner H-J (2008) Systematically convergent basis sets for explicitly correlated wavefunctions: The atoms H, He, B-Ne and Al-Ar. *J Chem Phys* 128:084102
55. Hill JG, Peterson KA (2014) Correlation consistent basis sets for explicitly correlated wavefunctions: Pseudopotential-based basis sets for the post-d main group elements Ga-Rn. *J Chem Phys* 141:094106
56. Kisiel Z, Pietrewicz BA, Fowler PW, Legon AC, Steiner E (2000) Rotational spectra of the less common isotopomers, electric dipole moment and double-minimum inversion potential of $\text{H}_2\text{O} \cdots \text{HCl}$. *J Phys Chem* 104:6970–6978
57. Davey JB, Legon AC, Thumwood JMA (2001) Interaction of water and dichlorine in the gas phase: an investigation of $\text{H}_2\text{O} \cdots \text{Cl}_2$ by rotational spectroscopy and ab initio calculations. *J Chem Phys* 114:6190–6202
58. Cooke SA, Cotti G, Evans CM, Holloway JH, Kisiel Z, Legon AC, Thumwood JMA (2001) Pre-reactive complexes in mixtures of water vapour with halogens: characterisation of $\text{H}_2\text{O} \cdots \text{ClF}$ and $\text{H}_2\text{O} \cdots \text{F}_2$ by a combination of rotational spectroscopy and ab initio calculations. *Chem Eur J* 7:2295–2305
59. Tyler JK, Sheridan J, Costain CC (1972) Microwave spectra of cyanamide-conclusions from μ_a transitions. *J Mol Spectrosc* 43:248–261
60. Mjoberg PJ, Almlöf J (1978) *Chem Phys* 29:201–208
61. Hill JG, Hu X (2013) Theoretical insights into the nature of halogen bonding in pre-reactive complexes. *Chem Eur J* 19:3620–3628
62. Bondi A (1964) van der Waals volumes and radii. *J Phys Chem* 68:441–451
63. Murray JS, Politzer P, Clark T (2010) Halogen bonding: an electrostatically driven highly directional non-covalent interaction. *Phys Chem Chem Phys* 12:7748–7757
64. Price SL, Stone AJ (1982) The anisotropy of the $\text{Cl}_2\text{-Cl}_2$ pair potential as shown by the crystal structure. Evidence for intermolecular bonding or lone pair effects? *Mol Phys* 47:1457–1470
65. Peebles SA, Fowler PW, Legon AC (1995) Anisotropic repulsion in complexes $\text{B} \cdots \text{Cl}_2$ and $\text{B} \cdots \text{HCl}$: the shape of the chlorine atom-in-a molecule. *Chem Phys Lett* 240:130–134
66. Legon AC, Millen DJ (1987) Hydrogen bonding as a probe for electron densities: limiting gas phase nucleophilicities and electrophilicities of B and HX. *J Am Chem Soc* 109:356–358

67. Legon AC (2014) A reduced radial potential energy function for halogen- and hydrogen-bonded complexes $B \cdots XY$ and $B \cdots HX$, where X and Y are halogen atoms. *Phys Chem Chem Phys* 16:25199–25199
68. Boys SF, Bernadi F (1970) The calculation of small molecular interactions by the differences of separate total energies. Some procedures with reduced errors. *Mol Phys* 19:553–566
69. Nagels N (2013) Building cryospectroscopic bridges: halogen bonding, hydrogen bonding and lone pair $\cdots \pi$ interactions. Ph.D. thesis, Departement Chemie, Universiteit Antwerpen
70. Hauchecorne D, Nagels N, van der Veken BJ, Herrebout WA (2012) $C-X \cdots \pi$ halogen and $C-X \cdots \pi$ hydrogen bonding: interactions of CF_3X (X=Cl, Br, I or H) with ethane and propene. *Phys Chem Chem Phys* 14:681–690
71. Valerio G, Raos G, Meille SV, Metrangolo P, Resnati G (2000) Halogen bonding in fluoroalkylhalides: a quantum chemical study of increasing fluorine substitution. *J Phys Chem A* 104:1617–1620